Palaeogeography, Palaeoclimatology, Palaeoecology 544 (2020) 109603

Contents lists available at ScienceDirect

Palaeogeography, Palaeoclimatology, Palaeoecology

journal homepage: www.elsevier.com/locate/palaeo

Changes in temperature and oxygen isotopic composition of Mediterranean water during the Mid-Pleistocene transition in the Montalbano Jonico section (southern Italy) using the clumped-isotope thermometer

Marion Peral[a,b,*], Dominique Blamart[a], Franck Bassinot[a], Mathieu Daëron[a], Fabien Dewilde[a,c], Helene Rebaubier[a], Sebastien Nomade[a], Angela Girone[d], Maria Marino[d], Patrizia Maiorano[d], Neri Ciaranfi[d]

[a] Laboratoire des Sciences du Climat et de l'Environnement, UMR8212, LSCE/IPSL, CEA-CNRS-UVSQ and University of Paris-Saclay, Gif-sur-Yvette, France
[b] School of Earth Science, University of Melbourne, 253-283 Elgin St, Carlton, VIC 3053, Australia
[c] Institut Universitaire Européen de la Mer, Université de Bretagne Occidentale, CNRS UMS3113, Place Nicolas Copernic, 29280 Plouzané, France
[d] Dipartimento di Scienze della Terra e Geoambientali, Università degli Studi di Bari Aldo Moro, via E. Orabona 4, 70125 Bari, Italy

ARTICLE INFO

Editor: Thierry Correge

Keywords:
Paleoceanography
MIS 19
MIS 31
Paleothermometry
Mg/Ca
Foraminifera
Stable isotope

ABSTRACT

Taking advantage of the recent clumped-isotope methodological developments, the present study focuses on the reconstruction of temperatures and seawater $\delta^{18}O$ in the central Mediterranean Sea across the Mid-Pleistocene section from Montalbano Jonico (south of Italy). Our results suggest that Mg/Ca paleothermometer can be biased over several intervals, making clumped-isotope a promising choice to reconstruct past changes in sea-water temperature and isotopic composition in the Mediterranean Sea. Our results provide the first clumped-isotope temperature and $\delta^{18}O_{SW}$ reconstruction across several glacial and interglacial Marine Isotope Stages from MIS 36 to MIS 19 in the central Mediterranean Sea.

During the climatic optimums of MIS 31 and MIS 19, considered as close analogues to the current interglacial in terms of insolation forcing, reconstructed average sub-surface temperatures from benthic foraminifer analyses (13.8 ± 1.5 °C and 14.8 ± 1.3 °C, respectively) and isotopic composition of seawater (between 1.6 ± 0.4‰ and 2.0 ± 0.3‰) are similar to the ones measured today below the thermocline in the Gulf of Taranto. Our results show that bottom water conditions remained similar in all the studied glacial periods, with cold temperatures around ~ 8 °C in average. The lack of a clear cooling across the Mid-Pleistocene either suggest that glacial oceanographic conditions in the Mediterranean Sea remained relatively stable between the 41 ka-world and the 100 ka-world or that the tectonic uplift that took place during this transition balanced out the MPT cooling trend through the shallowing of the deposition site.

1. Introduction

The Early- Mid-Pleistocene is a particularly puzzling time interval characterized by a major change in the frequency and amplitude of glacial-interglacial cycles, with a shift from low amplitude, obliquity-dominated climate changes (41 ka cycles) to larger amplitude ~ 100-ka dominated cycles (Ruddiman et al., 1986; Lisiecki and Raymo, 2005; Lang and Wolff, 2010; Head and Gibbard, 2015). This transition (Mid-Pleistocene Transition, noted MPT) corresponds to an intensification of glacial periods and an increase of their duration (Lisiecki and Raymo, 2005; Head and Gibbard, 2015 and references therein), with Marine Isotopic Stage (MIS) 22 being sometime considered as the precursor of glacial periods typical of the 100 ka-world. Paleo-temperature reconstructions are particularly important to better understand the Mid-Pleistocene evolution and try to disentangle the temperature from the ice volume effect in foraminifer $\delta^{18}O$ records. However, long time marine paleo-temperature reconstructions are rare across this period and several problems have been raised regarding usual paleo-thermometers. This is the case, in particular, for potential salinity and pH biases on the Mg/Ca paleo-thermometer (Mathien-Blard and Bassinot, 2009; Gray et al., 2018 and references therein), which cannot be dealt with easily for the MPT.

In the present study, we take advantage of the recently developed clumped isotope thermometry to reconstruct sea-water temperature

* Corresponding author at: School of Earth Science, University of Melbourne, 253-283 Elgin St, Carlton, VIC 3053, Australia
E-mail address: marion.peral@unimelb.edu.au (M. Peral).

https://doi.org/10.1016/j.palaeo.2020.109603
Received 26 April 2019; Received in revised form 13 January 2020; Accepted 13 January 2020
Available online 23 January 2020
0031-0182/

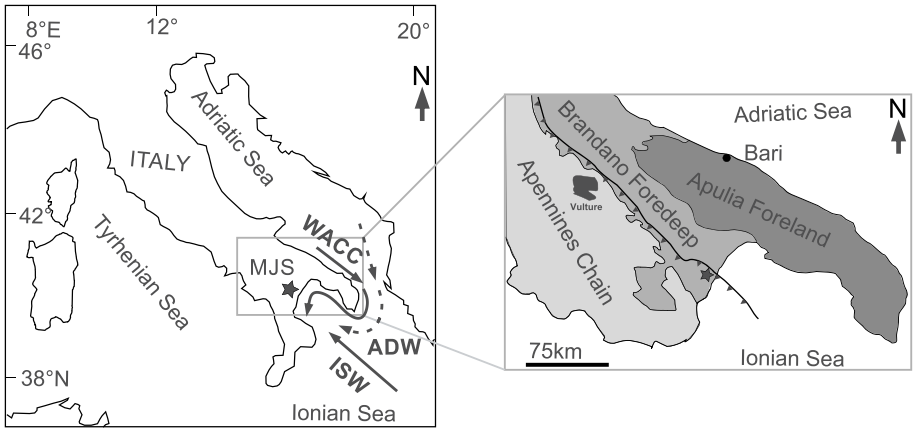

Fig. 1. General view of Italy with Montalbano Jonico location (MJS; black star) and Geological context.

and $\delta^{18}O$ changes across the MPT in the context of the Mediterranean Sea using the exposed Montalbano Jonico section (south Italy, Gulf of Taranto, central Mediterranean; Fig. 1). The carbonate clumped-isotope thermometer, noted Δ_{47} is based on the quantification of subtle statistical anomalies in the abundance of the doubly substituted carbonate isotopologue ($^{13}C^{18}O^{16}O^{16}O$) compared to a stochastic distribution of isotopes (Ghosh et al., 2006; Eiler, 2007; Eiler, 2011). For thermodynamical reasons, Δ_{47} varies with temperature (Schauble et al., 2006). As a result, the slightly higher abundance of $^{13}C–^{18}O$ bonds decreases systematically with mineral crystallisation temperature. The main advantages of the Δ_{47} thermometer compared to other more frequently used geochemical paleotemperature proxies (such as $\delta^{18}O$ and Mg/Ca) are the absence of detectable species-specific and salinity effects in both planktonic and benthic foraminifera (Tripati et al., 2010; Grauel et al., 2013; Peral et al., 2018) and the fact that it does not require any knowledge of seawater $\delta^{18}O$ (noted $\delta^{18}O_{SW}$ hereafter) in which the carbonate calcified (Schauble et al., 2006). Thus, combining Δ_{47} and $\delta^{18}O_C$ measurements in foraminifera allows reconstructing both past seawater temperatures and $\delta^{18}O_{SW}$.

We decided to focus our study on the exposed Montalbano Jonico section (MJS, south Italy, Gulf of Taranto, central Mediterranean; Fig. 1), which is one of the highest-resolution marine sedimentary record spanning the MPT (Bertini et al., 2015; Marino et al., 2015). Being a semi-enclosed basin, the Mediterranean Sea can amplify climate changes and its geographic position makes it sensitive to both tropical and high-latitude influences (Hurrell, 1995; Trigo et al., 2004; Giorgi, 2006; Lionello et al., 2006). Several studies have already revealed the clear imprint of MPT changes on the Mediterranean marine and continental environments (Joannin et al., 2008; Pol et al., 2010; Giaccio et al., 2015; Wagner et al., 2019). In the MJS, the benthic and planktonic $\delta^{18}O$ records show the clear alternation between glacial and interglacial periods, and a small enrichment of glacial benthic $\delta^{18}O$ across the MPT (Fig. 2; Brilli, 1998). There exists no accurately quantified-marine temperature and $\delta^{18}O_{sw}$ records over this key time interval yet. The exposed Montalbano Jonico section allows to collect large amounts of sedimentary material, which are necessary to replicate clumped-isotope analyses in order to reduce analytical uncertainties and provide the most accurate reconstruction possible of Δ_{47}-temperature changes along the Mid-Pleistocene of the central Mediterranean Sea.

2. Strategy and main objectives

When dealing with the Mid-Pleistocene interval, two periods are of particular interest: marine isotopic stages (MIS) 31 and 19. The MIS 31, also called “super interglacial” (Pollard and DeConto, 2009; DeConto et al., 2012; Melles et al., 2014; Coletti et al., 2015), extends from about 1.082 to 1.062 Ma (Lisiecki and Raymo, 2005). It is an unusually long interglacial for the 41 ka-world and numerous authors suggested that it could be a precursor of the high-amplitude ~ 100 ka cycles (e.g. Scherer et al., 2008; Girone et al., 2013). This interglacial is characterized by the highest summer insolation forcing of the Pleistocene (Laskar et al., 2004), while indirect pCO_2 reconstructions suggest concentration around 300 ppm at 1.0 Ma (Hönisch et al., 2009). In high latitudes and particularly in the North Atlantic, most of MIS 31 records point toward warm oceanic temperatures (Helmke et al., 2003; Bintanja et al., 2005; Bintanja and Van de Wal, 2008; Naafs et al., 2013), with differences, however, in the magnitude of this warming (Ruddiman et al., 1989; McClymont et al., 2008; Hillaire-Marcel et al., 2011; Oliveira et al., 2017). Several studies have focused on MIS 19 (Pol et al., 2010; Tzedakis et al., 2012; Giaccio et al., 2015; Maiorano et al., 2016; Nomade et al., 2019; Regattieri et al., 2019). They documented changes in the terrestrial and marine realms with continuous and high-resolution records and especially for the interglacial sensu-stricto (i.e. MIS 19c hereafter; Tzedakis et al., 2012; Giaccio et al., 2015; Sánchez-Goñi et al., 2016; Nomade et al., 2019). These records depict a shorter climatic optimum compared to MIS 31 (i.e. 10 ka up to 13 ka) followed by millennial- to-centennial-scale climate oscillations, particularly well-expressed within the substages 19a and 19b (Tzedakis et al., 2012; Giaccio et al., 2015; Sánchez-Goñi et al., 2016; Regattieri et al., 2018; Nomade et al., 2019).

The onset of these two interglacials are characterized by insolation forcing conditions that are relatively similar to those that prevailed during the onset of the Holocene (high obliquity, low precession), making these two MIS good candidates to study the response of the Mediterranean Sea under an orbital forcing similar to the Holocene but, presumably, under different mean climate conditions and greenhouse gas composition of the atmosphere.

The MJS is divided into two parts: Interval A (lower part of the section – 168 m thick, from MIS 37 to MIS 23) and Interval B (upper part of the section – 280 m thick; from MIS22 to the MIS17/16 transition), separated by a stratigraphic gap estimated to last about 19 ka (Ciaranfi et al., 2010; Fig. 2). As already mentioned above, available $\delta^{18}O$ data suggest a slight increase in glacial benthic $\delta^{18}O$ values between section A and section B, accompanied by an increase in the difference between planktonic and benthic $\delta^{18}O$ values. Such evolution does seem to be coherent with an intensification of glacials across the MPT. However, paleo-water depth reconstruction based on benthic foraminifer assemblages suggests that the depth of deposition of MJS varied from a bathyal environment in the Interval A to a circalittoral environment in the Interval B (Stefanelli, 2003). The transition from a deeper to a shallower environment appears relatively abrupt and synchronous to the stratigraphic gap observed between Intervals A and B, corresponding to the transition between MIS 23 – MIS 22 (Fig. 2; Stefanelli, 2003). This shallowing has been attributed to a tectonic

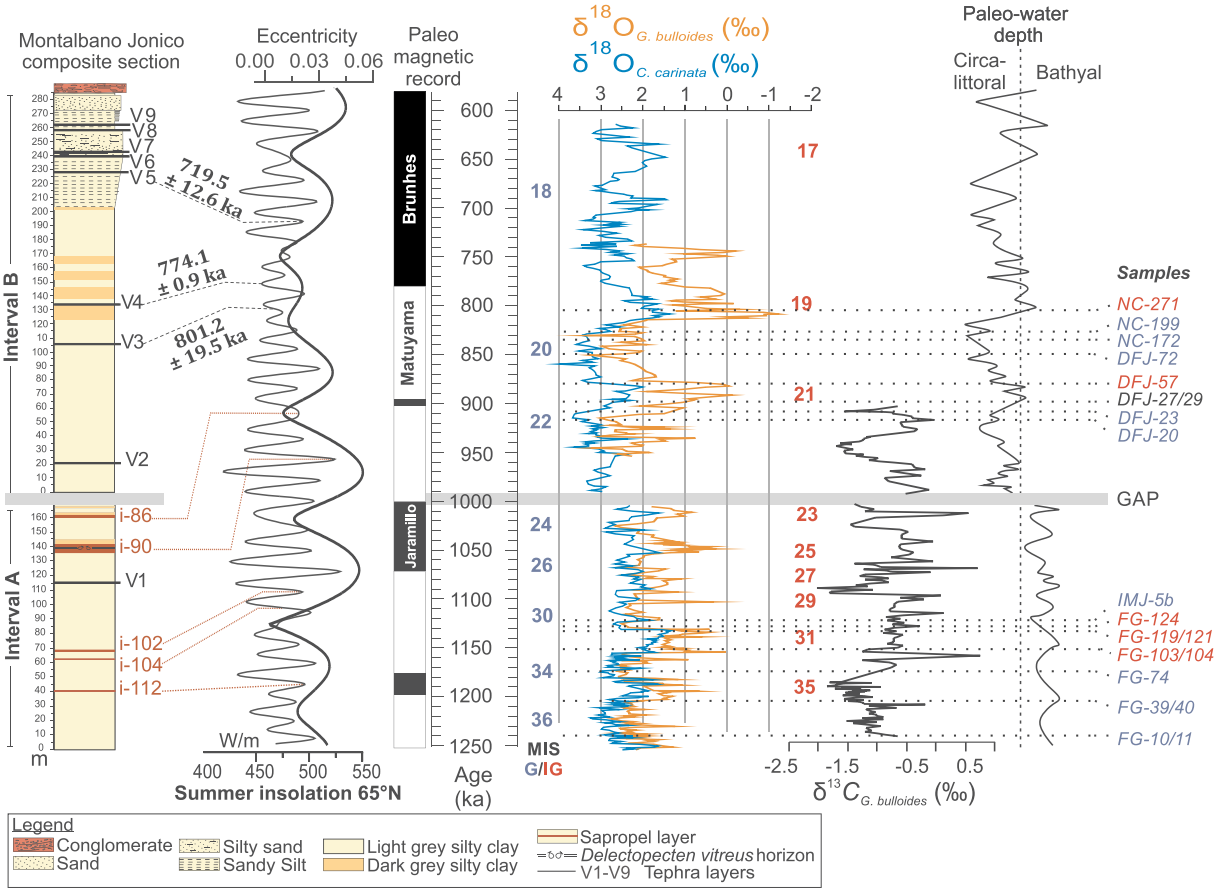

Fig. 2. Lithological and stratigraphical settings of MJ composite for Interval A and B. The composite is from Ciaranfi et al., 2010; the $\delta^{18}O_{G.\ bulloides}$ (planktonic foraminifera) and $\delta^{18}O_{benthic}$ (benthic foraminifera) curve are from Brilli, 1998; Brilli et al., 2000 and Ciaranfi et al., 2010. The $^{40}Ar/^{39}Ar$ ages of V3-V5 are in Ciaranfi et al., 2010; Maiorano et al., 2010; Petrosino et al., 2015; Simon et al., 2017 and Nomade et al., 2019. The correlation to sapropel stratigraphy was done according to Lourens (2004) and Konijnendijk et al. (2014). Summer insolation is from Laskar et al. (2004). The paleo-water depth was reconstructed in Stefanelli, 2003. G = glacials; IG = interglacials.

uplifting. The evolution of vertical $\delta^{18}O$ gradients (i.e. planktonic-benthic difference) and the slight increase in glacial benthic $\delta^{18}O$ across the MPT are counter-intuitive when considering that they took place during an important shallowing of the deposition site. In order to better constrain the relative importance of oceanographic and tectonic imprints in the Mid-Pleistocene evolution of glacial conditions recorded in MJS, we propose to separate temperature and $\delta^{18}O_{sw}$ effects in the benthic $\delta^{18}O$ record and compare the evolution of glacial periods from interval A (MIS 36, MIS 34 and MIS 30) with those from interval B (MIS 22 and MIS 20).

The present paper aims at two main objectives: 1) comparing the key MIS 31 and MIS 19 interglacials, and 2) documenting the evolution of the glacial conditions through the Mid-Pleistocene in the MJS. We achieve these goals by reconstructing seawater temperature through and oxygen isotope composition by combining clumped-isotope (Δ_{47}) temperature estimates and $\delta^{18}O$ measured in foraminifera. In addition, this work will compare Δ_{47}-derived temperatures in benthic foraminifera with Mg/Ca-derived temperatures.

Paleodepth reconstructions indicate that the water depth was only a few hundred meters at the time of deposition (D'Alessandro et al., 2003; Stefanelli, 2003; Aiello et al., 2015). Thus, benthic foraminifera in the MJS have recorded sub-surface conditions, characteristic of intermediate waters to upper deep waters. In the rest of this study, we will use the term, "subsurface water", for hydrographic conditions reconstructed from benthic foraminifers.

3. Regional settings and presentation of the Montalbano Jonico section

3.1. Modern oceanographic settings in the Gulf of Taranto

The Gulf of Taranto is a semi-enclosed basin, located in southern Italy and open to the Ionian Sea (Fig. 1). Its central depth exceeds 2000 m, while coastal areas (continental shelf) are shallower than 200 m. The surface circulation is connected to the Western Adriatic Coastal Current (WACC; Poulain, 2001; Bignami et al., 2007; Turchetto et al., 2007; Goudeau et al., 2014). The WACC has a relatively low salinity due to freshwater runoffs (Turchetto et al., 2007; Pinardi et al., 2016) and shows a clear intra-annual variability. Its influence in the Gulf of Taranto is weaker in summer than in winter and spring because of the reduced river discharges from the Po River and several Alpine and Apennine rivers, leading to a decreased inflow into the Gulf of Taranto during summer (Poulain, 2001; Milligan and Cattaneo, 2007; Brandimarte et al., 2011; Goudeau et al., 2014). In the Gulf of Taranto, waters from WACC are mixed with the Ionian Surface Water (ISW), from the central Ionian Sea (Poulain, 2001; Bignami et al., 2007; Turchetto et al., 2007; Goudeau et al., 2014). The Modified Levantine Intermediate Water (MLIW) can be traced in the basin between 200 and 600 m of water depth (Savini and Corselli, 2010). The deeper circulation (below 600 m) in the Gulf of Taranto is influenced by lateral water exchanges with Ionian and Adriatic Sea, which are affected by seasonal changes in the vertical stratification in response to changes in atmospheric dynamics (Turchetto et al., 2007; Civitarese et al., 2010; Cessi

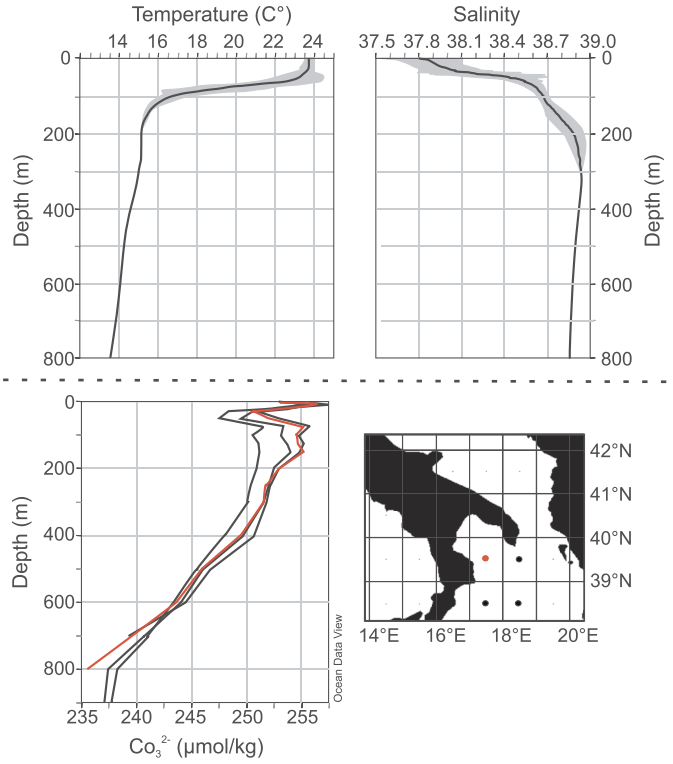

Fig. 3. Temperatures and salinity profiles from the Gulf of Taranto over the first 800 m (data from Pinardi et al., 2016 and World Ocean Atlas 2013); and $CO_3^{=}$ profile over the first 800 m at the entrance of the Gulf of Taranto (data from Goyet et al., 2000) in red, the closer station from our site location. (For interpretation of the references to colour in this figure legend, the reader is referred to the web version of this article.)

et al., 2014; Pinardi et al., 2016).

Today, surface-waters show an average temperature around 24 °C and a relatively low and constant salinity of 37.7, which result from the mix between the WACC and the ISW (Fig. 3; Poulain, 2001; Bignami et al., 2007; Turchetto et al., 2007; Goudeau et al., 2014; Pinardi et al., 2016). The annually-averaged thickness of the mixed-layer is ~ 50-60 m. The thermocline is abrupt, the temperatures decreasing rapidly from 23 to 24 °C at the base of the mixed layer (50-60 m) to around 16 °C at ~ 100 m (Fig. 3; Pinardi et al., 2016). The intermediate waters, between 100 and 300 m depth, show higher salinities and lower temperatures characteristic of the MLIW (Theocharis and Georgopoulos, 1993; Turchetto et al., 2007). The deeper-water mass shows a low, average temperature around of 14 °C, and a constant salinity of 39 (Fig. 3; Pinardi et al., 2016).

The carbonate ion concentration [$CO_3^{=}$] (Global Alkalinity and Total Dissolved Carbon Estimates Dataset, Goyet et al., 2000) varies from > 255 µmol/kg in surface waters to ~ 235 µmol/kg at the base of the 800 m profile shown in Fig. 3. These values are high, well above the equilibrium [$CO_3^{=}$] values for calcite (varying from 40 to 60 µmol/kg over this depth range), indicating that the entire water column is supersaturated with respect to calcite.

3.2. The Montalbano Jonico section

The Montalbano Jonico section (southern Italy; 40°17′27″N, 16°33′57″E), is located in the Lucania Basin of Bradano Trough (Balduzzi et al., 1982; Casnedi, 1988), between the external border of the Apennines fold and thrust belt and the internal margin of the Apulian Foreland (Fig. 1). The Bradano Trough formed in the Early Pliocene and evolved during the Pliocene and Pleistocene. Its inner border experienced deformation associated with polyphasic active thrusts, as a result of interactions between the Apulian Foreland and the Apennines Chain, which determined the north-eastward migration of the Cenozoic Apennine and Pliocene-Pleistocene foredeep units as well as the small-scale marine/lacustrine intramontane basins that were forming at that time (Patacca and Scandone, 2004). The outer margin of the Bradano Foredeep progressively overspread the Mesozoic-Cenozoic Apulian Foreland units (Casnedi et al., 1982).

The MJS comprises ~450-m-thick, upward-coarsening deposits ranging from hemipelagic silty clays to silty sands (Fig. 2 – Montalbano Jonico composite section). It is interspersed by nine volcanoclastic layers (labelled V1-V9) and five sapropel layers identifiable by benthic foraminiferal and macro-invertebrate assemblages (D'Alessandro et al., 2003; Stefanelli, 2003; Stefanelli et al., 2005; Maiorano et al., 2010).

The chronological framework of MJS is based on stable oxygen isotope measurements on benthic ($\delta^{18}O_b$; *Cassidulina carinata*) and planktonic ($\delta^{18}O_p$; *Globigerina bulloides*) foraminifera, combined with calcareous plankton biostratigraphy, radiometric dating ($^{40}Ar/^{39}Ar$) and identification of sapropel layers (Fig. 2). The whole series covers the interval from MIS 37 to MIS 17/16.

In the lower part of the section (Interval A; Fig. 2), an astronomical age-model was developed by tuning the sapropel layers to precession minima with a constant 3 ka time lag (Ciaranfi et al., 2010; Maiorano et al., 2010), while in the upper part of the section (Interval B; Fig. 2), the astronomical tuning was achieved by visual comparison of the MJS $\delta^{18}O_{planktonic}$ record to ODP Site 975 $\delta^{18}O_{planktonic}$ (Lourens, 2004). The tuning is also supported by glacial-interglacial oscillations observed in $\delta^{18}O_{benthic}$ at Montalbano Jonico that can be compared with open ocean benthic stack of Lisiecki and Raymo (2005). Additional tie-points were provided by tephras V3 and V5 precisely dated by $^{40}Ar/^{39}Ar$ (Ciaranfi et al., 2010; Maiorano et al., 2010; Petrosino et al., 2015). This chronostratigraphic frame indicates that the MJS covers the time interval from 1.240 to 0.645 Ma (Ciaranfi et al., 2010; Fig. 2). The estimated sedimentation rates range from 0.28 to 0.9 m/kyr for Interval A and from 0.5 to 2 m/kyr for Interval B (Ciaranfi et al., 2010; Maiorano et al., 2010). The chronostratigraphy of MIS20-MIS19 (belonging to Interval B, hereafter referred to as Ideal Section or IS) has been recently improved based on a much higher-resolution benthic foraminifer $\delta^{18}O$ record (~ 200 years resolution) and using a revised $^{40}Ar/^{39}Ar$ age of tephra V4 (Nomade et al., 2019).

3.3. Paleoenvironmental changes recorded in the MJS

3.3.1. Over the Interval A

The major paleoenvironmental changes that occurred during the Interval A of MJS spanning from 1.24 to 0.9 Ma (MIS 37 to 23), were orbitally controlled (Joannin et al., 2008; Girone et al., 2013). Sapropel-like horizons have been described in MJS and their occurrence has been explained by (i) the stratification of the water column and the preservation of organic material at the sea bottom and/or by (ii) enhanced sea surface productivity (Girone et al., 2013). The glacial interglacial cycles through Interval A were considered the result of complex interactions between global climate changes and regional/local responses.

In the MJS, MIS 31 limits were set at the mid-slope of MIS 32/31 and of MIS 31/30 transition in the benthic foraminifer $\delta^{18}O$ record, which correspond to 1.095 and 1.064 Ma respectively based on the age model of Maiorano et al. (2010). Based on calcareous nannofossil and planktonic foraminifera assemblages, it has been inferred that the MIS 31 corresponds to a long climatic optimum lasting 10 kyr, from 1.075 to 1.065 Ma (Girone et al., 2013). Micropaleontological and mineralogical data suggest warm and wet conditions associated with changes in the local precipitation regime with potential effects on sea surface temperature and salinity through enhanced freshwater input into the basin (Stefanelli, 2003; Joannin et al., 2008; Girone et al., 2013). The wet climate likely resulted from strong northern Hemisphere summer insolation associated to precession minimum in a period of high obliquity

and eccentricity. This warm climate phase coincided with regional tectonic instability that may have influenced local patterns of erosion and sediment transport (Girone et al., 2013), suggesting that paleoenvironmental changes over MIS 31 at MJS likely result from the interaction between global climate changes and regional factors, in particular associated to landscape evolution.

3.3.2. Over the Interval B

Interval B (MIS22-MIS17/16) had initially been studied at low resolution with a particular focus on time interval from MIS 20 to MIS 18 (Stefanelli, 2003, 2005; Aiello et al., 2015; Bertini et al., 2015; Toti, 2015; Marino et al., 2015; Maiorano et al., 2016). The chronostratigraphy of MIS 19 benefits from the precise and accurate $^{40}Ar/^{40}Ar$ age of the tephra layer V4 (Nomade et al., 2019) as well as from a high-resolution cosmogenic ^{10}Be profile (Simon et al., 2007), a proxy for the dipolar magnetic field intensity that makes it possible to clearly monitor the field weakening associated to the Brunhes-Matuyama magnetic reversal. It also benefits from recent, high-resolution studies of marine microfossils and pollen assemblages (Aiello et al., 2015; Bertini et al., 2015; Marino et al., 2015; Maiorano et al., 2016), and from high-resolution records of benthic $\delta^{18}O$ and $\delta^{13}C$ changes recently obtained over the MIS 20-MIS 18 interval (Nomade et al., 2019). This set of data provides invaluable pieces of information about the climatic and environmental variability throughout the MIS 19.

The deglaciation between MIS 20 and MIS 19 (Termination IX) is characterized by the cyclic advection of cold surface waters that likely originated from the North Atlantic and resulted in an "Heinrich-like event" followed by a potential "Bølling-Allerød-like event" and a "Younger Dryas-like event" (Maiorano et al., 2016). During MIS19c, several proxies point to the existence of a shallow-water analogue to a sapropel event (Maiorano et al., 2016). This so-called "red interval" or "ghost sapropel" (Emeis et al., 2000), seems to correspond to the "i-cycle 74" event according to Lourens (2004). The existence of a shallow-water sapropel is supported (i) by a negative excursion in benthic foraminifera $\delta^{13}C$, which suggests an enhanced stratification of the upper water column and/or an increased productivity (Nomade et al., 2019), and which is coeval with (ii) a low oxygen content at the sediment-water interface (Stefanelli, 2003). During this event, marine (Maiorano et al., 2016) and continental (Bertini et al., 2015) proxies suggest an increase in sea-surface temperatures (SST) and a climatic amelioration on land with a rapid increase in annual precipitation, both of which providing favourable conditions for sapropel formation during an insolation maximum (Maiorano et al., 2016; Nomade et al., 2019). The MIS 19c is associated with warm and wet conditions in continual and warm surface waters (Bertini et al., 2015; Maiorano et al., 2016; Nomade et al., 2019).

4. Materials and methods

4.1. Conventional stable isotope analyses

Planktonic and benthic foraminifera were handpicked for stable isotope analyses. Around 20–30 individuals of *Globigerinoides ruber* and *Cassidulina carinata* and 7–15 individuals for *Uvigerina mediterranea* and *Elphidium crispum*, were picked from the 200–355 µm fraction. The three-benthic species (*U. mediterranea*, *C. carinata* and *E. crispum*) are shallow infaunal or epifaunal species (Altenbach et al., 1999; Fontanier et al., 2002; Murray, 2006), which can live on different substrates, such as on sand or on algae (Murray, 1963). From 1 to 5 replicate analyses of $\delta^{18}O$ and $\delta^{13}C$ were performed. Foraminifera were cleaned in an ultrasonic bath for few seconds with reagent-grade methanol to eliminate impurities. $\delta^{18}O_{VPDB}$ and $\delta^{13}C_{VPDB}$ values were measured at the Laboratoire des Sciences du Climat et de l'Environnement (LSCE) using a MultiCarb system coupled to a dual-inlet Isoprime (Elementar). Standardization to VPDB was based on repeated measurements of international reference materials NBS 19 and NBS 18, with respective nominal values for $\delta^{18}O_{VPDB}$ of - 2.20‰ and - 23.01‰, and for $\delta^{13}C_{VPDB}$ of 1.95‰ and - 5.01‰. The uncertainties reported here are based on the external reproducibility of an in-laboratory carbonate standard (MARGO) with 1SD = 0.05‰ for $\delta^{18}O_{VPDB}$ and 1SD = 0.03‰ for $\delta^{13}C_{VPDB}$.

4.2. Clumped-isotope analyses

Clumped-isotope method is a promising isotopic thermometer for seawater paleo-reconstructions because 1) it does not require that one knows the past isotopic composition of sweater, $\delta^{18}O_{SW}$ (Schauble et al., 2006) and 2) there are no detectable vital or salinity effects for both the planktonic and the benthic foraminifera Δ_{47} (Tripati et al., 2010; Grauel et al., 2013; Peral et al., 2018). The main limitation is analytical. From 2 to 3 mg of foraminifer calcite are required in order to perform one clumped isotope measurement and a minimum of four replicates are mandatory to reduce significantly the analytical uncertainty. In the Montalbano Jonico section, large amounts of thick and heavy benthic foraminifer shells were available for Δ_{47} replicate analyses, but planktonic foraminifera were not present in large enough quantities to reconstruct SST with the clumped-isotope thermometer.

A total of 257 clumped-isotope analyses were performed at the LSCE, including 143 measurements on benthic foraminifera from Interval A and B, and 114 measurements of carbonate standards. We combined different foraminifer size fractions and cleaned benthic foraminifera with water and methanol after crushing, following the protocol described by Peral et al. (2018). Each carbonate sample was then weighed and between 2 and 3 mg were dissolved in a common phosphoric acid bath at 90 °C during 15 min. The resulting CO_2 was purified in an automated line by cryogenic trapping to remove water and passed through a Porapak Q column at −20 °C under helium 6.0 flow. This CO_2 was transferred by gas expansion into an Isoprime 100 dual-inlet mass spectrometer (Daëron et al., 2016). Conversion of Δ_{47}^{raw} to absolute Δ_{47} values was done using carbonate standards (ETH-1/2/3; Meckler et al., 2014; Bernasconi et al., 2018), and processed using the IUPAC isotopic parameters (Brand et al., 2010) following the procedure described by Daëron et al. (2016). "Absolute" Δ_{47} values were then converted to temperatures using the calibration of Peral et al. (2018).

Where possible, three species of benthic foraminifera were picked from each sample (i.e. same stratigraphic depth), *Uvigerina mediterranea* (200–355 µm), *Cassidulina carinata* (200–315 µm) and *Elphidium crispum* (200–450 µm; only for one stratigraphic level). From 2 to 27 replicates for each sample/species pair were done in 4 sessions of measurements between July 2016 and June 2018. The first session (2016–07) and the last one (2018–05) were corrected for a slow trend observed in the measured Δ_{47} values of ETH-3, probably resulting from subtle changes in the ion collector backgrounds. Each analytical session (defined as continuous period of Δ_{47} measurements) was assigned an independent external Δ_{47} reproducibility (respectively 15.9 ppm, 13.9 ppm, 20.9 ppm and 18.1 ppm at 1SE) based on repeated analyses of standards and samples. Details about the data processing are given with the python routine provided in the supplementary material.

4.3. Analyses of Mg/Ca ratio

Mg/Ca measurements were performed at LSCE on planktonic and benthic foraminifera. A minimum of 30 foraminifera (~ 250 µg) were hand-picked in the size range between 250 and 355 µm and cleaned following the Barker et al. (2003) protocol. Shells were crushed between two glass plates and the resulting fragments were put into microvials, making it possible to wash out fine material (i.e. clay) through repeated cleaning with purified water and then ethanol. In order to remove potential organic contaminants, the samples were then oxidized with alkali-buffered 1% H_2O_2 solution for 10 min at 100 °C. The final cleaning treatment consists in a rapid leaching with 0.001 M HNO_3. After dissolution in HNO_3 0.075 M, each sample was analysed by

inductively coupled plasma mass spectrometry (ICP-MS), using a PlasmaQuant ELITE system from Analytik Jena. After a preliminary run to estimate the Ca concentrations, samples were then diluted to a uniform Ca concentration of around 100 ppm. Mg/Ca ratios were accurately determined following the intensity ratio method (De Villiers et al., 2002). The calibration standards were prepared from single element solutions (e.g. Ca, Sr, Mg). Mg/Ca instrumental precision was determined based on multiple replicates of a standard solution of known Mg/Ca composition. It averages ± 1.3%, with daily variations varying from 0.9 to 1.6%.

The Mg/Ca ratios were measured on the planktonic foraminifera *G. ruber* and on the benthic foraminifera *U. mediterranea*. The Mg/Ca ratios were converted to temperature using species-specific calibrations:

- For *G. ruber*: we used the calibration of Anand et al. (2003)

$$T = \log\left(\left(\frac{Mg/Ca}{0.449\ (\pm 0.06)}\right)/0.09\right) \quad (1)$$

- For *U. mediterranea*: we used the calibration of Elderfield et al. (2010)

$$T = \log\left(\left(\frac{Mg/Ca}{0.86\ (\pm 0.05)}\right)/0.07\ (\pm 0.005)\right) \quad (2)$$

where T (in °C) is the temperature.

The uncertainties were calculated by propagating the analytical errors, based on the long-term standard deviation of our standards and uncertainties associated with calibrations.

4.3.1. Calibration and potential biases

Several potential sources of uncertainties or leading to systematic errors have been reported for Mg/Ca-thermometry in foraminifer shells. First, Mg/Ca-T calibration exercises have revealed species-dependent differences and/or size effects for foraminifers (Anand et al., 2003) and inter-laboratory comparisons have shown the existence of significant offset (up to 14%) associated to the cleaning protocol (Rosenthal et al., 2004). Thus, in the present work, we have used species-specific Mg/Ca-T calibrations that were obtained with the same cleaning protocol that we used (i.e. Anand et al., 2003 for *G. ruber* in the 250-350 µm size fraction, and Elderfield et al., 2010 for *U. mediterranea*).

Recent calibrations have also suggested that Mg/Ca in foraminifer shells is not only temperature dependent but could be also affected by salinity (Nürnberg et al., 1996; Lea et al., 1999; Ferguson et al., 2008; Kisakürek et al., 2008; Mathien-Blard and Bassinot, 2009; Arbuszewski et al., 2010; Gray et al., 2018) and/or pH or $CO_3^=$ (Russell et al., 2004; Kisakürek et al., 2008; Elderfield et al., 2006; Gray et al., 2018). However, because we cannot estimate accurately salinity and pH variations along the MPT interval, no effort was made in the present paper to take these effects into account.

5. Results

5.1. $\delta^{18}O_{vpdb}$ measurements

$\delta^{18}O_{VPDB}$ and $\delta^{13}C_{VPDB}$ measurements were performed on 3 species of benthic (*Cassidulina carinata, Elphidium crispum* and *Uvigerina mediterranea*) and one species of planktonic foraminifera (*Globigerinoides ruber*), except for sample DFJ-27/29 (transition between MIS 22 and MIS 21) and the older two samples (FG-39/40 and FG-10/11) in which *G. ruber* specimens were not present in sufficient quantity. All the measurements are presented in supplementary material Table S1.

The difference of $\Delta^{18}O_c$ between the three species of benthic foraminifera ranges between 0 and 0.43‰ (Table 1), which is larger than the internal analytical uncertainty (± 0.05‰). Since the good reproducibility of replicate measurements suggests homogeneous samples, the observed differences likely result from the so-called "vital" effects. But our results are puzzling since, according to Grossman (1987), both *Uvigerina* spp. and *Cassidulina* ssp. are believed to precipitate following the equation of Kim and O'Neil (1997). The range of differences and the small number of intervals studied here do not allow us to quantify precisely the species-specific, oxygen-18 differences between *C. carinata*, *U. mediterranea* and *E. crispum*.

Variations in the difference between benthic species and the planktonic species *G. ruber* ($\Delta^{18}O_{c\ (p\ vs\ b)}$, hereafter) are larger than the inter-benthic variability, and are, as expected, primarily driven by changes in the planktonic $\delta^{18}O$ values. $\Delta^{18}O_{c\ (p\ vs\ b)}$ values remain relatively constant for glacial periods (MIS 36, 34, 30 and 20), hovering between 1.37 and 1.86‰, except for sample DFJ-23 (MIS 22), which yields ~ 2.5‰, a value comparable to those for interglacial periods. By contrast, a much larger variability is observed for the interglacial periods (MIS 31, 21 and 19), with benthic-planktonic differences ($\Delta^{18}O_{c\ (p\ vs\ b)}$) ranging between 1.32 and 3.19‰ (Table 1).

5.2. Temperatures estimated from clumped-isotope measurements

Final Δ_{47} values and the corresponding temperature reconstructions are given in Table 2. More details in the data processing (python code) and all the Δ_{47} measurements are presented in supplementary material Table S2. Given the analytical standard deviation, the Δ_{47}-derived temperatures for *U. mediterranea* and *C. carinata* are statistically indistinguishable from each other in samples NC-199, DFJ-57, FG-39/40 and FG-10/11. The absence of species-specific effects in clumped isotopes (Tripati et al., 2010; Grauel et al., 2013; Peral et al., 2018) allows us to combine results from the three benthic species to compute average Δ_{47}-derived temperatures and reduce the analytical error. By doing so, we assume that there is no significant temperature difference between the water-sediment interface (epifaunal species habitat) and the first centimetres of sediments where the infaunal species grew. An additional assumption is that bioturbation does not result in large vertical remobilisation that could have brought together benthic specimens from different climatic intervals. The high sedimentation rates of MJS and the large quantity of material required for Δ_{47} measurements insure that the effects of vertical remobilisation can be neglected.

The reconstructed glacial temperatures range from 7.1 °C (± 3.6 °C, 2SE) to 12.1 °C (± 4.2 °C, 2SE), for samples NC-172, DFJ-72, DFJ-23, DFJ-20, FG-103/104 and FG-124, while interglacial temperatures are warmer, with a lower variability, respectively 14.8 °C (± 2.6 °C, 2SE) and 16.6 (± 3 °C, 2SE) for MIS 19 (sample NC-271) and MIS 21 (DFJ-57). Surprisingly, two of the three Δ_{47}-derived temperature values obtained during MIS31 (samples FG-103/104 and FG-119/121) are similar to the glacial period temperatures and only the last sample (FG-124), within the $\delta^{18}O$ optimum of MIS31, shows a warm temperature of 13.8 °C (± 3 °C, 2SE). It is worth noting that samples DFJ-27-29 and NC-172, located at the transitions between MIS 22 – MIS 21 and between MIS 20 – MIS 19, yield significantly different temperatures, 8.6 °C (± 3.8 °C, 2SE) and 12.1 °C (± 1.6 °C, 2SE; Table 2), respectively.

5.3. Temperatures estimated from Mg/Ca ratio measurements

Our study makes it possible to compare Mg/Ca-thermometry to clumped-isotope paleotemperatures. All the Mg/Ca analyses on benthic foraminifers were performed on the species *U. mediterranea*. For a few samples in which enough planktonic shells were available, we also reconstructed Mg/Ca-derived sea-surface temperatures (SST hereafter) using the planktonic foraminifer *G. ruber*. All the Mg/Ca results are provided in supplementary material Table S3 and summarized in Table 3.

Monitoring Al/Ca, Fe/Ca and Mn/Ca makes it possible to check for potential contaminations. The low values Mn/Ca and Al/Ca and the lack of any clear correlation between these elemental ratios and Mg/Ca

Table 1
Difference (absolute values in ‰, PDB) of $\delta^{18}O$ between each species.

Samples	MIS	$\Delta^{18}O$ (‰) *C. carinata – U. mediterranea*	$\Delta^{18}O$ (‰) *E. crispum – C. carinata*	$\Delta^{18}O$ (‰) *E. crispum – U. mediterranea*	$\Delta^{18}O$ (‰) *E. crispum – G. ruber*	$\Delta^{18}O$ (‰) *U. mediterranea - G. ruber*	$\Delta^{18}O$ (‰) *C. carinata – G. ruber*
NC-271	19	0.13				2.57	2.44
NC-199	20/19	0.25	0.18	0.43	1.9	2.33	2.08
NC-172	20	0.02				1.64	1.62
DFJ-72	20	0.07				1.49	1.56
DFJ-57	21	0.19				2.30	2.11
DFJ-27/29	22/21	0.00					
DFJ-23	22	0.32				2.67	2.35
DFJ-20	22	0.15				1.83	1.68
IMJ-5b	30	0.24				1.86	1.62
FG-124	31	0.05				2.50	2.45
FG-119/121	31	0.29				1.61	1.32
FG-103/104	31	0.07				3.19	3.13
FG-74	34	0.14				1.50	1.37
FG-39/40	36	0.30					
FG-10/11	36	0.08					

values (Fig. 4) suggest that our Mg/Ca dataset is neither affected by Mn-rich oxides nor clay material. Only one sample (DFJ-72) showed an unusually high Al/Ca ratio, but it is not associated with an anomalous Mg/Ca ratio (Fig. 4). The Fe/Ca values are relatively high in our samples (Fig. 4), but without any noticeable impact on Mg/Ca. We suspect that the Fe values could reflect the presence of small amounts of pyrite, which is not removed by our cleaning protocol. Sample FG-119/121 was analysed twice because the first results yielded an unrealistic benthic Mg/Ca-temperature of 28.6 °C (± 3.4 °C, 2SE), warmer than the Mg/Ca-derived SST obtained in the same sample on *G. ruber* (22.7 ± 1.8 °C, 2SE; Table 3). Although there was no indication of detrital or oxide contamination, we decided to re-analyse this sample after adding another leaching step to our cleaning protocol. The second set of replicates yield a bottom water temperature of 20.9 °C (± 3.0 °C, 2SE) for this sample.

Through the Interval A, as expected, Mg/Ca-derived SSTs indicate colder temperatures during the glacials MIS 36 (FG-10/11 and FG-39/40), MIS 34 (FG-74) and MIS 30 (IMJ-5b) than during interglacial MIS 31 (FG-103/104, FG-119/121 and FG-124). Along the interglacial MIS 31, SSTs increase from 22.5 to 24.7 °C. As far as benthic foraminifer results are concerned, glacial Mg/Ca-derived sub-surface water temperatures are in good agreement with our Δ_{47}-derived temperature estimates. By contrast, in interglacial MIS 31, Mg/Ca-derived temperatures obtained from *U. mediterranea* are higher than the corresponding Δ_{47}-derived temperatures.

In the Interval B, Mg/Ca-SSTs vary less in Interval B than interval A, ranging between 20.8 °C (± 1.8 °C, 2SE) and 23.1 °C (± 1.6 °C, 2SE). Two samples, however, show much warmer temperatures: NC-199 (transition from MIS 20 and 19), with a SST of 27.8 °C (± 1.8 °C, 2SE) and sample NC-271 (MIS 19) with a SST of 25.4 °C (± 1.6 °C, 2SE; Table 3). As far as bottom water temperature are concerned, Mg/Ca-reconstructed temperatures range from 9.7 to 18.2 °C. Surprisingly, the glacial periods yield warmer bottom temperatures than the interglacials: the two glacial MIS 22 samples yield high bottom temperatures of 18.2 °C (± 2.6 °C, 2SE) and 17.2 °C (± 2.4 °C, 2SE), and in MIS 20 bottom temperatures are 14.1 °C and 14.7 °C (± 2.2 °C, 2SE). The deglaciation samples show Mg/Ca temperatures comparable to those derived from Δ_{47}, with 9.7 °C (± 1.8 °C, 2SE) for MIS 22–21 and 14.7 °C

Table 2
$\delta^{18}O_{VPDB}$, $\delta^{13}C_{VPDB}$, Δ_{47} values and temperatures derived from Δ_{47} values for each sample within each species.*

Sample	Species	MIS	N	$\delta^{13}C_{VPDB}$ (‰)	SE	$\delta^{18}O_{VPDB}$ (‰)	SE	Δ_{47}	SE	T-Δ_{47} (°C)	SE
NC-271	*C. carinata*	19	5	−0.68	0.03	1.96	0.06	0.713	0.007	13.3	2.0
	U. mediterranea	19	8	−0.48	0.02	2.00	0.05	0.705	0.006	15.7	1.6
	Combined*	19	13	−0.55	0.02	1.98	0.04	0.708	0.004	14.8	1.3
NC-199	*C. carinata*	20/19	6	−0.29	0.02	3.57	0.05	0.718	0.006	11.8	1.8
	Elphidium crispum	20/19	27	0.95	0.01	3.53	0.02	0.717	0.003	12.2	0.9
	Combined*	20/19	33	0.78	0.01	3.54	0.02	0.717	0.003	12.1	0.8
NC-172	*C. carinata*	20	4	−0.62	0.01	3.75	0.04	0.736	0.007	7.1	1.8
DFJ-72	*C. carinata*	20	4	−0.59	0.01	3.50	0.04	0.731	0.007	8.4	1.9
DFJ-57	*C. carinata*	21	3	−0.59	0.03	2.35	0.06	0.693	0.007	19.2	2.1
	U. mediterranea	21	5	−0.51	0.03	2.33	0.06	0.710	0.007	14.1	2.0
	Combined*	21	10	−0.55	0.02	2.34	0.04	0.701	0.005	16.6	1.5
DFJ-27/29	*U. mediterranea*	22/21	4	−0.43	0.01	2.94	0.04	0.730	0.007	8.6	1.9
DFJ-23	*C. carinata*	22	4	−0.63	0.01	3.21	0.04	0.727	0.007	9.4	1.9
DFJ-20	*C. carinata*	22	5	−0.63	0.03	2.94	0.08	0.717	0.009	12.1	2.6
IMJ-5b	*U. mediterranea*	30	15	−0.44	0.01	3.45	0.02	0.732	0.005	8.0	1.2
FG-124	*U. mediterranea*	31	11	−0.58	0.01	2.19	0.03	0.711	0.005	13.8	1.5
FG-119/121	*U. mediterranea*	31	12	−0.43	0.01	2.21	0.03	0.732	0.005	8.1	1.3
FG-103/104	*U. mediterranea*	31	12	−0.83	0.01	2.75	0.03	0.735	0.005	7.1	1.2
FG-74	*U. mediterranea*	34	2	−0.52	0.04	3.61	0.09	0.728	0.011	9.2	3.0
FG-39/40	*C. carrinata*	36	4	−0.82	0.03	3.51	0.06	0.716	0.010	12.6	2.9
	U. mediterranea	36	4	−0.71	0.01	3.77	0.04	0.737	0.007	6.7	1.8
	Combined*	36	27	−0.72	0.01	3.68	0.03	0.731	0.006	8.4	1.5
FG-10/11	*C. carrinata*	36	4	−0.59	0.03	3.17	0.06	0.712	0.010	13.5	2.9
	U. mediterranea	36	4	−0.57	0.01	3.34	0.04	0.724	0.007	10.3	1.9
	Combined*	36	5	−0.57	0.01	3.28	0.03	0.720	0.006	11.2	1.6

* Combined: mix of different benthic species.

Table 3
Mg/Ca values and temperatures derived from Mg/Ca values for each samples and species.

Samples	MIS	N	Mg/Ca	Species	T-Mg/Ca (°C)	SE
NC-271	19	1	4.41	*G. ruber*	25.4	0.8
NC-199	20/19	1	2.93		20.8	0.8
NC-172	20	1	5.46		27.8	0.9
DFJ-72		1	2.94		20.9	0.9
DFJ-57	21	1	3.59		23.1	0.8
DFJ-23	22	1	3.35		22.3	0.9
DFJ-20	20/19	1	2.94		20.9	0.8
IMJ-5b	30	1	2.41		18.7	0.9
FG-124	31	1	4.14		24.7	0.8
FG-119/121		1	3.45		22.7	0.9
FG-103/104		1	3.51		22.9	0.9
FG-74	34	1	2.70		19.9	0.8
NC-271	19	1	1.96	*U. mediterranea*	12.9	0.8
NC-199	20/19	1	2.09		14.7	1.1
NC-172	20	1	2.09		14.7	1.1
DFJ-72	22	1	2.04		14.1	1.1
DFJ-57	21	1	1.89		11.9	0.7
DFJ-27/29	22/21	1	1.74		9.7	0.9
DFJ-23	22	1	2.26		17.2	1.2
DFJ-20	20	1	2.33		18.2	1.3
IMJ-5b	30	1	1.54		6.9	0.8
FG-124	31	1	2.26		17.1	0.9
FG-119/121		1	3.06		28.6	1.7
FG-119/121		1	2.52		20.9	1.5
FG-103/104		1	1.94		12.6	1.0
FG-74	34	1	1.73		9.6	0.7
FG-39/40	36	1	1.63		8.1	0.8
FG-10/11		1	1.60		7.8	0.8

(± 2.2 °C, 2SE) for MIS 20–19. Bottom water temperatures for interglacial periods are indistinguishable, within analytical uncertainties, from Δ_{47}-derived estimates: 11.9 °C (± 1.4 °C, 2SE) for MIS 21 and 12.9 °C (± 1.6 °C, 2SE) for MIS 19 (Table 3).

5.4. Subsurface seawater $\delta^{18}O$ reconstruction

The subsurface seawater $\delta^{18}O$ ($\delta^{18}O_{SW}$, hereafter) derived from paired Δ_{47}-$\delta^{18}O_C$ data are presented in Table 4. We paired our Δ_{47}-derived temperature estimates with the corresponding $\delta^{18}O_C$ values of each benthic species, using the $^{18}O/^{16}O$ fractionation relationship of Kim and O'Neil (1997):

$$1000 \ln(\alpha cc/w) = 18.03 \times 1000/T - 32.17 \quad (3)$$

where T is temperature in ° Kelvin (K) and αcc/w is the oxygen-18 fractionation factor between calcite and water: $\alpha cc/w = (1 + \delta^{18}O_{C/VSMOW}/1000)/(1 + \delta^{18}O_{SW/VSMOW}/1000)$ with $\delta^{18}O_{C/VSMOW}$ and $\delta^{18}O_{SW/VSMOW}$ corresponding to foraminiferal calcite and seawater, respectively, both relative to VSMOW.

Reconstructed $\delta^{18}O_{SW}$ values range from 0.7‰ (± 0.6‰ 2SE) to 3.0‰ (± 0.4‰ 2SE), with higher values during glacials than during interglacials through the Interval A. Within MIS 31 the $\delta^{18}O_{SW}$ values are relatively low (1.0‰ ± 0.6‰, 2SE) for sample FG-103/104, and 0.7‰ (± 0.6‰, 2SE) for sample FG-119/121 but increase to 2.0‰ (± 0.6‰, 2SE) in sample FG-124. In the interval B, changes between interglacial and glacial periods are small and remain within the range of propagated analytical uncertainties.

6. Discussion

6.1. Clumped isotope versus Mg/Ca-derived temperatures

As indicated above, the comparison of the two thermometers can only be achieved for benthic foraminifers since we could not extract enough planktonic shells for clumped-isotope analyses. Within Interval A of MJS, throughout the three glacial periods we investigated, both

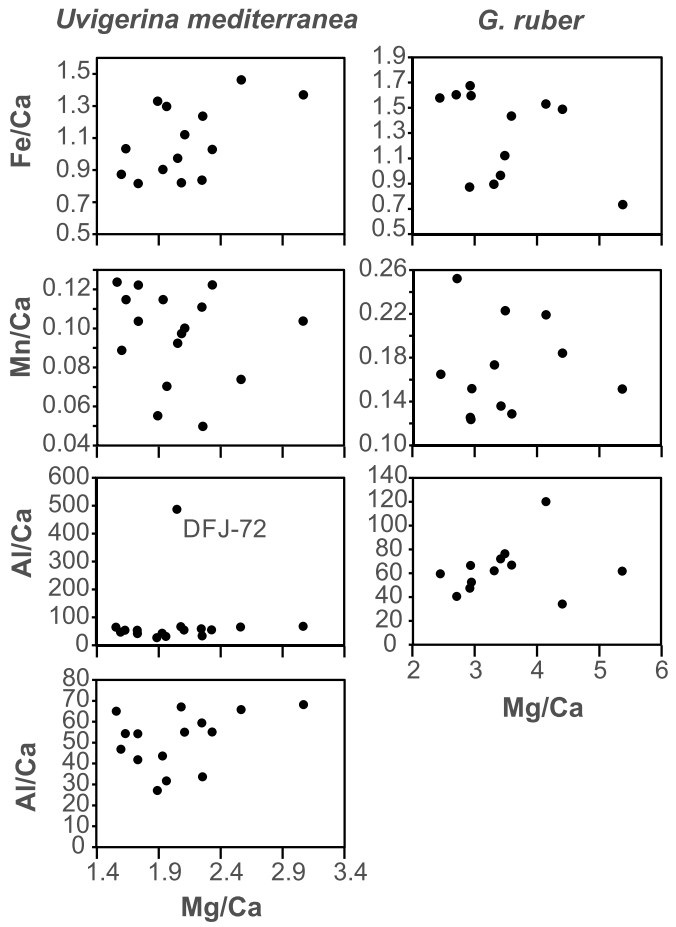

Fig. 4. Fe-, Mn- and Al/Ca ratio alongside Mg/Ca for all of our benthic sample (*Uvigerina mediterranea*; first column) and planktonic (*G. ruber*; second column). The last box represents Al/Ca versus Mg/Ca for the benthic measurement without the sample DFJ-72, which present a very high value of Al/Ca.

thermometers yield very similar temperature estimates (Fig. 5.a). By contrast, during interglacial MIS 31, Mg/Ca-derived temperatures are significantly higher than those derived from Δ_{47}. The first set of analyses on sample FG-119/121 (MIS 31) resulted in an unrealistic benthic Mg/Ca-derived temperature (28.6 ± 3.4 °C, 2SE), warmer than the Mg/Ca-derived SST values obtained in the same sample on *G. ruber* (22.7 ± 1.8 °C, 2SE; Table 3). We re-analysed this sample and the second set of data yielded a cooler benthic temperature (20.9 ± 3.0 °C 2SE), although still much warmer than the corresponding Δ_{47} estimate (8.1 ± 2.6 °C 2SE).

For the Interval B, the Mg/Ca-derived temperatures do not show significant changes between glacial and interglacial periods (Fig. 5.b). By contrast, Δ_{47} temperatures display larger variations correlated with benthic foraminifer $\delta^{18}O$ oscillations. The Mg/Ca-derived temperatures are higher than the Δ_{47}-derived ones during glacial periods, and lower during interglacial periods.

The Mg/Ca-derived temperatures during glacials such as for instance those in MIS22 (i.e. 18.2 ± 2.6 °C (2SE) and 17.2 ± 2.4 °C (2SE)) are not only higher than Δ_{47} results, they also correspond to temperatures only found today at very shallow water depths (~ 100 m) in the Gulf of Taranto (Pinardi et al., 2016; Fig. 3). The difference between benthic and planktonic $\delta^{18}O$ (which vary from $\Delta\delta^{18}O_{c\ (p\ vs\ b)} = 1.75$ to $\Delta\delta^{18}O_{c\ (p\ vs\ b)} = 2.51$ in interval B) rule out the possibility that the deposition site could have been located under such a shallow water depth. As seen above, trace elements, used to monitor potential contaminations (i.e. Mn, Fe, Al), do not reveal any oxides contamination or presence of detrital material. Even sample FG-119/121, for

Table 4
$\delta^{18}O_{SW}$ records derived from paired Δ_{47}-$\delta^{18}O_C$ in benthic foraminifera, using the O-isotopic fractionation factor at equilibrium of Kim and O'Neil (1997).

Samples	MIS	Species	T-Δ_{47} (°C)	SE	δ^{18}Oc (‰)	SE	δ^{18}Osw (‰)	SE
NC-271	19	*C. carinata*	13.3	2	1.96	0.06	1.6	0.4
NC-271		*U. mediterranea*	15.7	1.6	2	0.05	2.2	0.4
NC-199	20/19	*C. carinata*	11.8	1.8	3.57	0.05	2.9	0.4
NC-199		*E. crispum*	12.2	0.9	3.53	0.02	3.0	0.2
DFJ-72	20	*C. carinata*	8.4	1.9	3.5	0.04	2.0	0.4
NC-172		*C. carinata*	7.1	1.8	3.75	0.04	2.1	0.4
DFJ-57	21	*C. carinata*	19.2	2	2.35	0.06	3.3	0.4
DFJ-57		*U. mediterranea*	14.1	2.1	2.33	0.06	2.2	0.4
DFJ-27/29	22/21	*U. mediterranea*	8.6	1.9	2.94	0.04	1.6	0.4
DFJ-20	22	*C. carinata*	12.1	2.6	3.21	0.04	2.0	0.4
DFJ-23		*C. carinata*	9.4	1.9	2.94	0.08	2.3	0.6
IMJ-5b	30	*U. mediterranea*	8.0	1.2	3.45	0.02	1.9	0.3
FG-124	31	*U. mediterranea*	13.8	1.5	2.19	0.03	2.0	0.3
FG-119/121		*U. mediterranea*	8.1	1.3	2.21	0.03	0.7	0.3
FG-104		*U. mediterranea*	7.1	1.2	2.75	0.03	1.0	0.3
FG-74	34	*U. mediterranea*	9.2	3.0	3.61	0.09	2.4	0.7
FG-39/40	36	*C. carinata*	12.6	2.9	3.51	0.06	3.0	0.6
		U. mediterranea	6.7	1.8	3.77	0.04	1.9	0.4
FG-10/11		*C. carinata*	13.5	2.9	3.17	0.06	2.9	0.6
		U. mediterranea	10.3	1.9	3.34	0.04	2.3	0.4

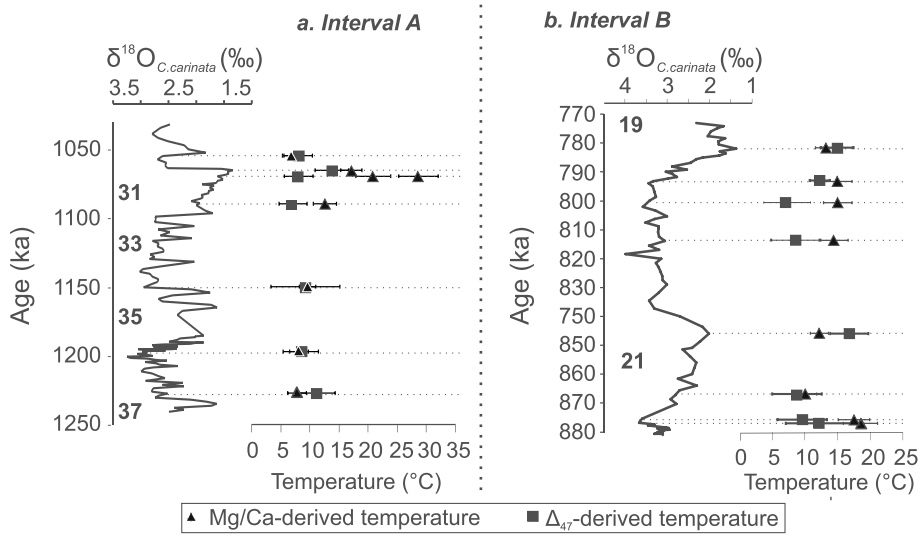

Fig. 5. comparison of Δ_{47}- (in scare) and Mg/Ca-derived (in triangle) temperatures (2SE), performed on benthic foraminifera (*U. mediterranea*) through Interval A (a.) and Interval B (b.) at MJS, associated to $\delta^{18}O_{bentic}$ (Brilli, 1998).

which a first set of results yielded a clearly anomalous bottom water temperature of 28.7 °C (± 3.4 °C, 2SE; warmer than the Mg/Ca-derived surface temperature obtained on the same sample) did not show anomalous Mn, Fe or Al contents (Fig. 4).

It has been shown from recent studies of core-top material that the Mg/Ca-thermometer in the Mediterranean Sea can be affected by the growth of Mg-rich calcite precipitated on foraminifer shells during early diagenetic processes (Boussetta et al., 2011; Sabbatini et al., 2011). The development of diagenetic calcite has been attributed to the super-saturation of Mediterranean bottom water [$CO_3^{=}$] with respect to calcite. However, if such a diagenetic mechanism was at play, it would affect both benthic and planktonic shells. In general, Mg/Ca-derived temperatures performed on planktonic shells do not result in unrealistic SST values (assuming that past values should be in the same range as modern values), with the exception of sample NC-172. Thus, it is not clear whether anomalous Mg/Ca-derived sub-surface temperatures could be attributed to a diagenetic effect. Alternatively, several studies have concluded that the Mg/Ca-thermometer on foraminifers can be biased by salinity and/or pH (Russell et al., 2004; Elderfield et al., 2006; Raitzsch et al., 2008; Kisakürek et al., 2008; Mathien-Blard and Bassinot, 2009; Gray et al., 2018). Modern geochemical profiles show that $CO_3^{=}$ concentrations in the Gulf of Taranto (and in most of the Mediterranean Sea) are much higher than in open ocean areas (Fig. 3). Yet, without estimates of pH or [$CO_3^{=}$] variations along the Mid-Pleistocene in the Mediterranean Sea one has no possibility to conclude about pH or carbonate ion influences on the Mg/Ca-thermometer in MJS. As far as a potential salinity effect is concerned, benthic-derived $\delta^{18}O_{SW}$ values from paired Δ_{47}-$\delta^{18}O$ do not show a clear relationship with Mg/Ca-temperatures but uncertainties are too large to drive any robust conclusion.

One cannot exclude also the possibility that the Mg/Ca ratio of waters in the Gulf of Taranto did not remain constant through time owing to the semi-enclosed nature of the basin, which may make it sensitive to continental rock weathering and local river runoffs. The Mg/Ca-thermometry is based on the assumption that Mg/Ca in sea-water is constant and invariant through time. This assumption is likely to be true in open oceans due to the long residence time of Mg and Ca, respectively 13 Ma and 1 Ma (Broecker and Peng, 1982; Bruland, 1983; Riley and Skirrow, 1975). However, seawater Mg/Ca may have varied through time in the Gulf of Taranto due to local inputs of dissolved Mg

and Ca from nearby river runoffs. Why such changes may have affected preferentially sub-surface Mg/Ca records is not clear, though, and we have no possibility to address that potential source of bias for Mg/Ca-thermometry.

In conclusion, we cannot rule out the possibility that discrepancies we observed in several intervals between benthic Mg/Ca- and Δ_{47}-derived temperatures reflect changes in the chemistry of bottom waters and/or diagenetic effects but given the observation available in the present paper none of the above hypotheses can be tested with confidence. Further studies are mandatory to address those anomalously high Mg/Ca-derived sub-surface temperatures in MJS. For the rest of this manuscript, we have decided to favour Δ_{47}-derived subsurface temperatures for our palaeoceanographic interpretations owing to the fact that in the present state of our current knowledge, there is no strong bias known for the clumped-isotope thermometer whereas several studies have highlighted potential problems for the Mg/Ca-thermometry in the Mediterranean Sea (Ferguson et al., 2008; Boussetta et al., 2011; Sabbatini et al., 2011). But those issues about Mg/Ca biases are not agreed upon by the whole community, several recent works concluding about the quality and consistency of Mg/Ca-derived temperatures in the Mediterranean Sea (e.g. Cisneros et al., 2015; Català et al., 2019).

In the present paper, although we favour clumped-isotope temperatures for benthic foraminifers, we have no alternative than using Mg/Ca-derived temperatures for sea-surface conditions (planktonic data).

6.2. Paleoceanographic conditions during the glacial periods

We propose firstly to describe the evolution of the glacial periods through the MPT at MJS (Fig. 6) in term of water-column stratification and sub-surface water temperatures and $\delta^{18}O_{SW}$. To the best of our knowledge, our results provide the first sub-surface temperature and $\delta^{18}O_{SW}$ reconstructions for the five Mid-Pleistocene glacial periods MIS 36, 34, 30, 22 and 20 in the central Mediterranean Sea.

6.2.1. Glacial conditions within Interval A

Δ_{47}-derived temperature estimates are low (between 8.0 °C ± 2.4 °C and 11.2 °C ± 3.2 °C at 2SE; Table 2; Fig. 6) within the Interval A. Such values are much cooler than temperatures that can be found today in the upper water column of the Gulf of Taranto (Pinardi et al., 2016, Fig. 3).

Paired Δ_{47}-$\delta^{18}O$ data obtained on specific-benthic species were used to reconstruct past $\delta^{18}O$ of sub-surface seawater. As expected, the glacial seawaters are oxygen-18-enriched relative to the interglacial MIS 31 values, likely reflecting the fact that more water is stored in continental ice sheets during these glacial periods than during MIS 31 (Fig. 6).

The difference of $\delta^{18}O_c$ between the surface (planktonic foraminifera) and sub-surface (benthic foraminifera; $\Delta^{18}O_{c\ (p\ vs\ b)}$) can be used to address the vertical stratification (Zahn et al., 1991). Lower $\Delta^{18}O_{c\ (p\ vs\ b)}$ values are observed for glacial periods (MIS 34 and 30) compared to those for MIS 31, which argues for a more efficient vertical mixing during glacial periods (Fig. 6).

The reconstructions of land conditions are based on pollen and can be summarized by the use of the ratio between two groups of taxa: mesothermic and steppic taxa. This ratio makes it possible to discriminate between warm-temperate periods (mesothermic dominance) and cold periods (steppic dominance; Fig. 7; Joannin et al., 2008). One of the most abundant local taxa is the mesophilous deciduous tree *Quercus*, which is also the most representative taxon of the mesothermic plants recorded through the Interval A (Joannin et al., 2008). This taxon suggests that warm-temperate periods are also humid (Rossignol-Strick and Paterne, 1999). Several warm/temperate and wet phases characterized by the dominance of mesothermic groups are highlighted during the interglacial periods through the Interval A, while the glacial periods are characterized by much colder and drier climates (i.e. dominance of steppic elements; Fig. 7). Changes in the relative abundance of tropical-subtropical marine planktonic species (Fig. 7; Girone et al., 2013) suggest that warm surface conditions (i.e. increased abundance of *G. ruber* and *Globigerinoides tenellus*) were associated to warm periods on land (Joannin et al., 2008), and drifted slowly to cooler conditions at the onset of glacial periods. The glacial MIS 30 is characterized by an abrupt decrease of tropical-subtropical planktonic species indicating colder conditions (Fig. 7; Girone et al., 2013), compared to the previous warm MIS 31. The evolution of the mesothermic vs. steppic ratio suggests cold and dry climate that may have significantly reduced the river runoff and resulted in saltier waters in the Gulf of Taranto (high $\delta^{18}O_{SW}$; Fig. 6), thus making the upper water column more prone to vertical mixing during the glacial periods. This agrees with the higher glacial $\delta^{13}C_{planktonic}$ values which may reflect increased surface productivity made possible by the enhanced vertical mixing and the upward redistribution of nutrient-enriched sub-surface waters (Fig. 2; Brilli, 1998).

6.2.2. Glacial conditions within Interval B

The two samples from MIS 22 provide contrasting pieces of information despite having been retrieved close to one another in the MJS. The older sample (DFJ-20) is characterized by a relatively warm sub-surface Δ_{47}-temperature (12.1 ± 5.2 °C at 2 SE) (Fig. 6). For this stratigraphic level, the $\Delta^{18}O_{c\ (p\ vs\ b)}$ is small, suggesting a good vertical mixing (Fig. 6). The second sample (DFJ-23), retrieved in the peak maximum of $\delta^{18}O$, reveals a colder sub-surface Δ_{47}-temperature (9.4 ± 1.9 °C). In this sample, $\Delta^{18}O_{c\ (p\ vs\ b)}$ is high, implying a more pronounced stratification of the water column (Fig. 6). Changes in sub-surface temperature reconstructed from benthic Δ_{47} appear coherent with vertical mixing history reconstructed from $\Delta^{18}O_{c\ (p\ vs\ b)}$, with lower sub-surface temperature when stratification is stronger and higher sub-surface temperature associated to more active vertical mixing. Yet, one cannot rule out the possibility that sub-surface temperature history is also controlled to some extent by lateral advection of thermocline water of Ionian or Adriatic origins (Pinardi et al., 2016).

The glacial MIS 20 is characterized by cold, sub-surface Δ_{47}-derived temperatures and some vertical mixing of the column water (as evidenced by the low $\Delta^{18}O_{c\ (p\ vs\ b)}$ gradient; Fig. 6). These observations, combined with the constant and high value of $\delta^{18}O_b$ (Fig. 8; Nomade et al., 2019), suggest that the climatic conditions during the MIS 20 were relatively cold and stable. The late MIS 20 (change between samples NC-172 and NC-199) corresponds to a − 0.25‰ decrease of $\delta^{18}O_{benthic}$ (Fig. 8). This would be equivalent to a temperature increase of ~ 1 °C, assuming a constant $\delta^{18}O_{SW}$. However, clumped isotopes indicate that the bottom water temperatures increased by ~ 5 °C (Figs. 6 and 8) between the two studied samples. This implies that the shift in $\delta^{18}O_b$ actually reflects the combined effects of a temperature increase and a 1‰ increase of water $\delta^{18}O_{SW}$. SSTs derived from foraminiferal and nannofossil assemblages (PC1 nannofossil and foraminifera) suggest persistent and cold surface water temperatures across the MIS 20 (Fig. 8). These low temperatures are evidenced by the high abundance of the polar-subpolar species *Neogloboquadrina pachyderma* left coiling (Fig. 8) and *Coccolithus pelagicus* ssp. *pelagicus* (Maiorano et al., 2016). The strong stratification that persisted despite the relative warming of sub-surface temperatures suggests that the increase of $\delta^{18}O_{SW}$ could correspond to the lateral advection of saltier (and warmer) sub-surface water at the end of MIS 20.

6.2.3. Evolution of glacial conditions through the Mid-Pleistocene Transition

As seen above, in interval A the glacial periods we studied show similar conditions characterized by high $\delta^{18}O_{SW}$ (~ 1.7‰) and cold (~ 9 °C) sub-surface temperatures in a context of well-mixed water column (Fig. 6). In Interval B, glacial periods are slightly more variable (Fig. 6). The hydrographic conditions during MIS 20 are similar to those

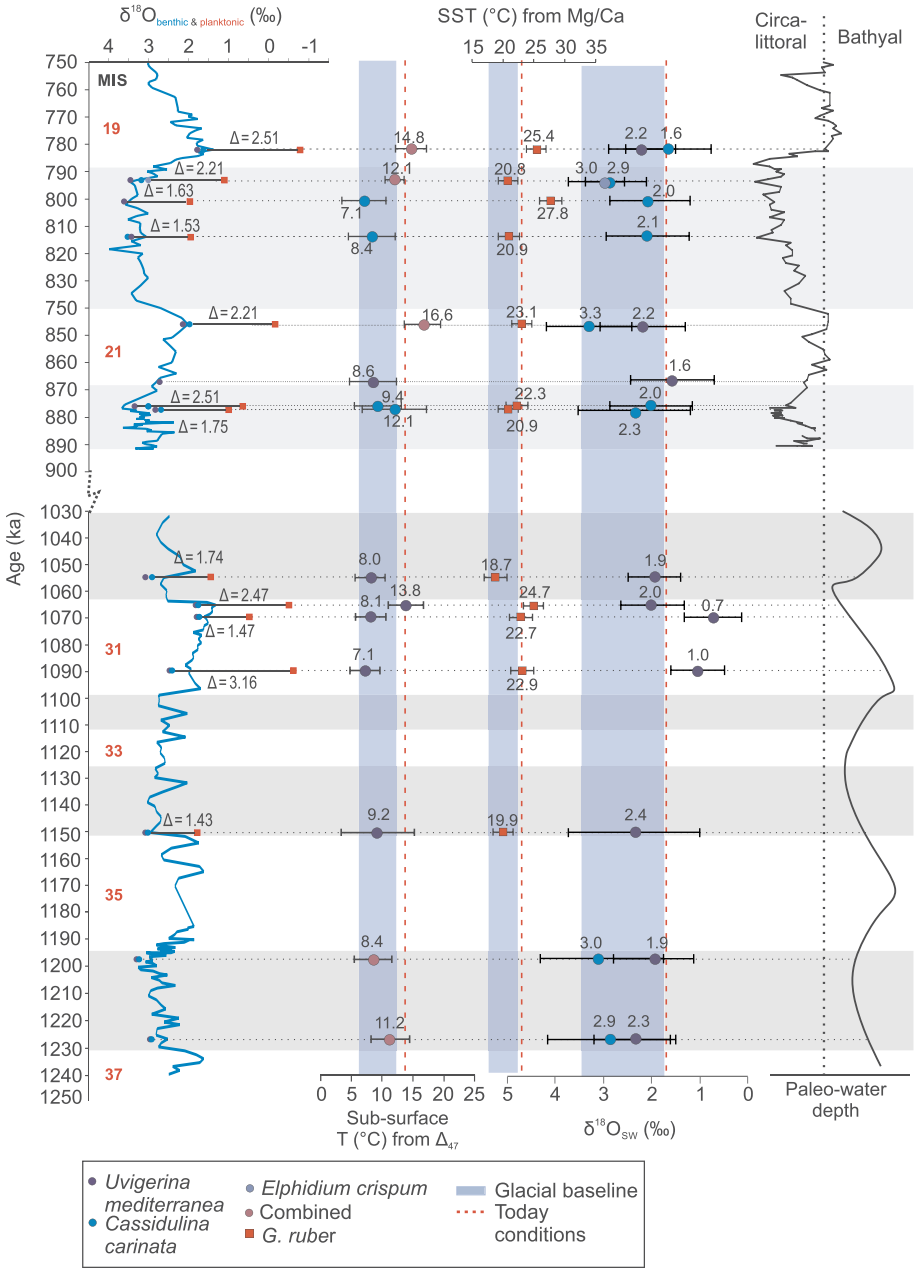

Fig. 6. Synthesis of main results for Interval A and B of MJS with $\delta^{18}O$ curve from benthic foraminifera (Brilli, 1998), our $\Delta\delta^{18}O$ between benthic and planktonic foraminifera, Δ_{47}-derived subsurface temperatures, Mg/Ca-derived SST, reconstructed subsurface $\delta^{18}O_{SW}$ (‰, VSMOW) and the reconstructed paleo-water (Stefanelli, 2003). All uncertainties are at 2SE.

occurring during glacial periods of Interval A. The two nearby samples analysed in MIS 22 suggest, however, the possibility of some variability during glacials with the penultimate MIS22 sample showing a surprisingly warmer temperature (12.1 °C) than the MIS22 sample that was retrieved in the maximum $\delta^{18}O$ peak (9.4 °C; Fig. 6). When averaging out these two MIS22 temperatures, the mean value is slightly higher than in the other glacials studied in MJS. While the MIS22 is often seen in many open ocean $\delta^{18}O$ records as one of the first intense post-MPT glacials, it seems to be characterized by anomalously warmer sub-surface temperatures compared to other Mid-Pleistocene glacial periods in the Gulf of Taranto (Fig. 6).

The paleo-water depth reconstruction (Fig. 6) suggests that water depth varied from bathyal through Interval A to circalittoral through Interval B due to tectonic uplifting (Stefanelli, 2003). If the structure of the water column had remained roughly similar to today, we would expect that such a major shallowing of the deposition site would have resulted in much warmer sub-surface (benthic) temperatures and reduced planktonic-benthic differences. This is not what is observed in the data. Within the limit of our error uncertainties, sub-surface (benthic) water temperatures and $\delta^{18}O_{SW}$ appear to be rather constant and undistinguishable between all the studied glacials throughout intervals A and B (with the exception of one sample in MIS22). The absence of any clear temperature increase may either suggest that the tectonic uplift was more limited than previously thought and/or that the benthic temperature increase resulting from the shallowing of the site had been counterbalanced by an overall cooling of the water column in interval B compared to interval A.

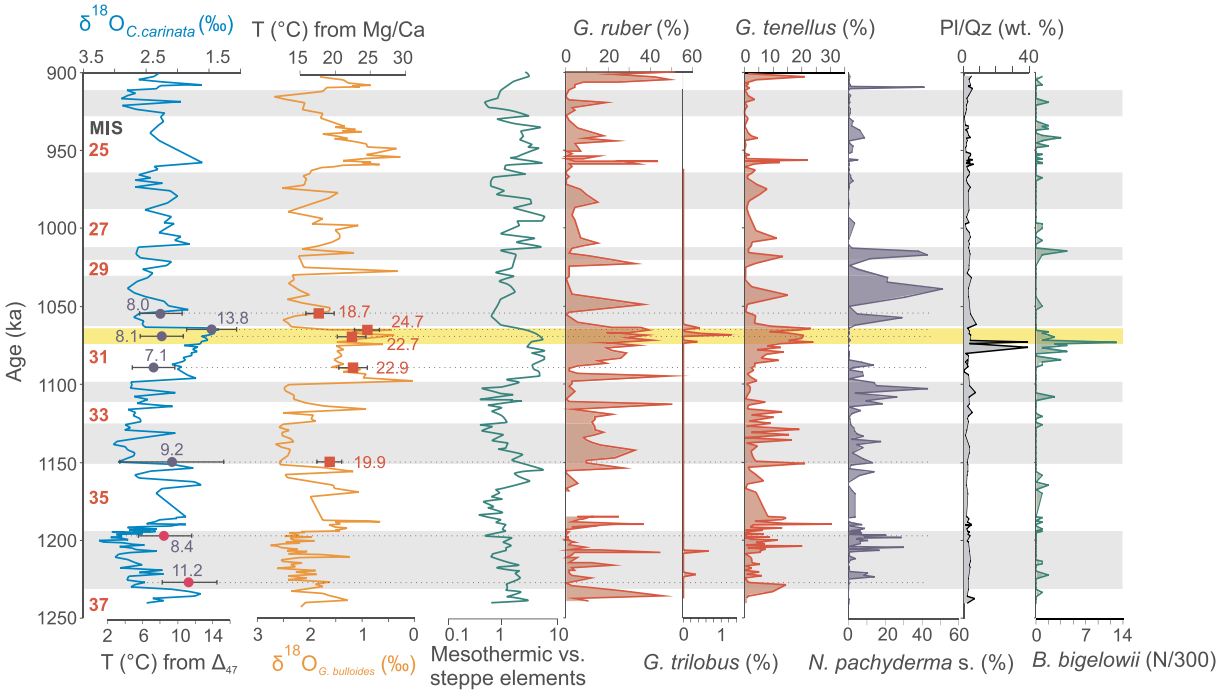

Fig. 7. $\delta^{18}O$ curves of benthic and planktonic foraminifera through the Interval A of MJS from 1.25 to 0.9 Ma (Brilli, 1998; Brilli et al., 2000; Ciaranfi et al., 2010) with our subsurface Δ_{47}- and surface Mg/Ca-derived temperatures, the ratio mesothermic vs steppe elements (Joannin et al., 2008), calcareous planktonic foraminifer abundances (red = "warm" species; bleu = "cold" species), *B. begelowii* abundance and plagioclase/quartz ratio (Girone et al., 2013). Gray bands correspond to glacial periods and yellow band to the climatic optimum of MIS 31. (For interpretation of the references to colour in this figure legend, the reader is referred to the web version of this article.)

6.3. Paleoceanographic conditions during the interglacial periods

We focused on three interglacial periods: (i) MIS 31 and MIS 19 - because they are potential analogues to Holocene in terms of orbital parameters - and (ii) MIS 21 - because it is pivotal in the MPT, occurring just after glacial MIS22. Interestingly, the deglaciation episodes leading to these three interglacials present strong differences. Termination XV (MIS 32–31) is characterized by an abrupt decrease of benthic foraminifer $\delta^{18}O_C$, while the two others (terminations X-MIS22/21 and IX – MIS20/19) are more gradual (Fig. 6). Furthermore, the beginning of the transitions to MIS 31 and the MIS 21 show relatively cold subsurface water conditions, while the sub-surface water at MIS 20/19 transition is warmer (Fig. 6).

As seen above, our data suggest that Δ47-derived sub-surface temperatures remained surprisingly cold during most of MIS31 (around 7–8 °C), similar to glacial temperatures, and only increased during the optimum of MIS31. We have no analytical reason to reject these values, yet they provide very puzzling pieces of information about sub-surface conditions during MIS31. Combining these low temperatures with the corresponding δ^{18}Oc values result in seawater δ^{18}Oc that are much lower in the lower part of MIS31 (i.e. 1.0‰ ± 0.6‰ and 0.7‰ ± 0.6‰ at 2SE, respectively) than any of the other intervals studied in MJS. The subsurface $\delta^{18}O_{SW}$ at the beginning of MIS 31 are low (1.0‰ ± 0.6‰ and 0.7‰ ± 0.6‰ at 2SE). Such values could be attributed to a combination of global signal (decrease of ice-sheet volume) and regional processes (enhancement of runoff around the Mediterranean Sea and/or incursion of North Atlantic water; Fig. 6). Enhancement of runoff is supported by micropaleontological and sedimentary data, which suggest a strong input of freshwater and the increase of the detrital component from land, evidenced respectively by a peak in the high relative abundance *Braarudosphaera bigelowii*, a low-salinity nannofossil species, and high Pl/Qz ratios (Fig. 7; Girone et al., 2013).

During MIS19, strong vertical stratification is associated to the deposition of a sapropel-like event (Nomade et al., 2019). No sapropel-like layer has been found at MJS during MIS 31, whereas in the Mediterranean Sea, the sapropel i-100 was deposited during this interval. Further studies will be necessary to decipher whether specific conditions blocked the deposition of a carbon-rich material in the Southern Apennines foredeep during MIS 31.

The MIS 22/21 transition has been poorly documented at MJS in previous studies and we cannot confront our data with other indicators. The MIS 20/19 transition, on the opposite, has been extensively studied. Previous works have shown that the deglaciation was characterized by several noticeable events: 1) the incursion of cold waters from the North Atlantic resulting a thermic evolution typical of a *Heinrich-like* episode, with moderately cold SST (PC1 nannofossils and foraminifera, abundance of *N. pachyderma* left coiling in Fig. 8), followed by a sharp interval of low SSTs (Maiorano et al., 2016), and 2) the deposition of a sapropel-like event (Maiorano et al., 2016), corresponding to a strong stratification of the water column (high $\Delta^{18}O_{c\ (p\ vs\ b)}$, and low $\delta^{13}C_{benthic}$ from Nomade et al., 2019). Another possible source of freshwater could be sub-surface waters from Adriatic origin that could gain their low $\delta^{18}O_{SW}$ signature from the melting of Alpine glaciers.

Our data indicate that the climatic optimum occurred at the end of both MIS 31 and MIS 21, whereas it occurred at the beginning of the interglacial interval for MIS 19. The MIS 31 covers two precession-cycles, the climate optimum being associated with the second precession-related peak of summer insolation (Fig. 2). This climatic optimum shows a sub-surface temperature of 13.8 °C ± 3 °C (2SE), whereas it is 14.8 ± 2.6 °C (2SE) for MIS19. Among the three interglacials studied, MIS 21 shows the highest sub-surface temperature: 16.6 °C ± 3 °C (2SE). All interglacial periods following MIS 19, also show their climatic optimum associated to the first strong precession-related summer insolation peak. Furthermore, we observed increase in $\delta^{18}O_{SW}$ during the climate optimum of MIS 31, with similar values to those recorded at the climatic optimum for interglacials MIS 21 and MIS 19. It is worth to

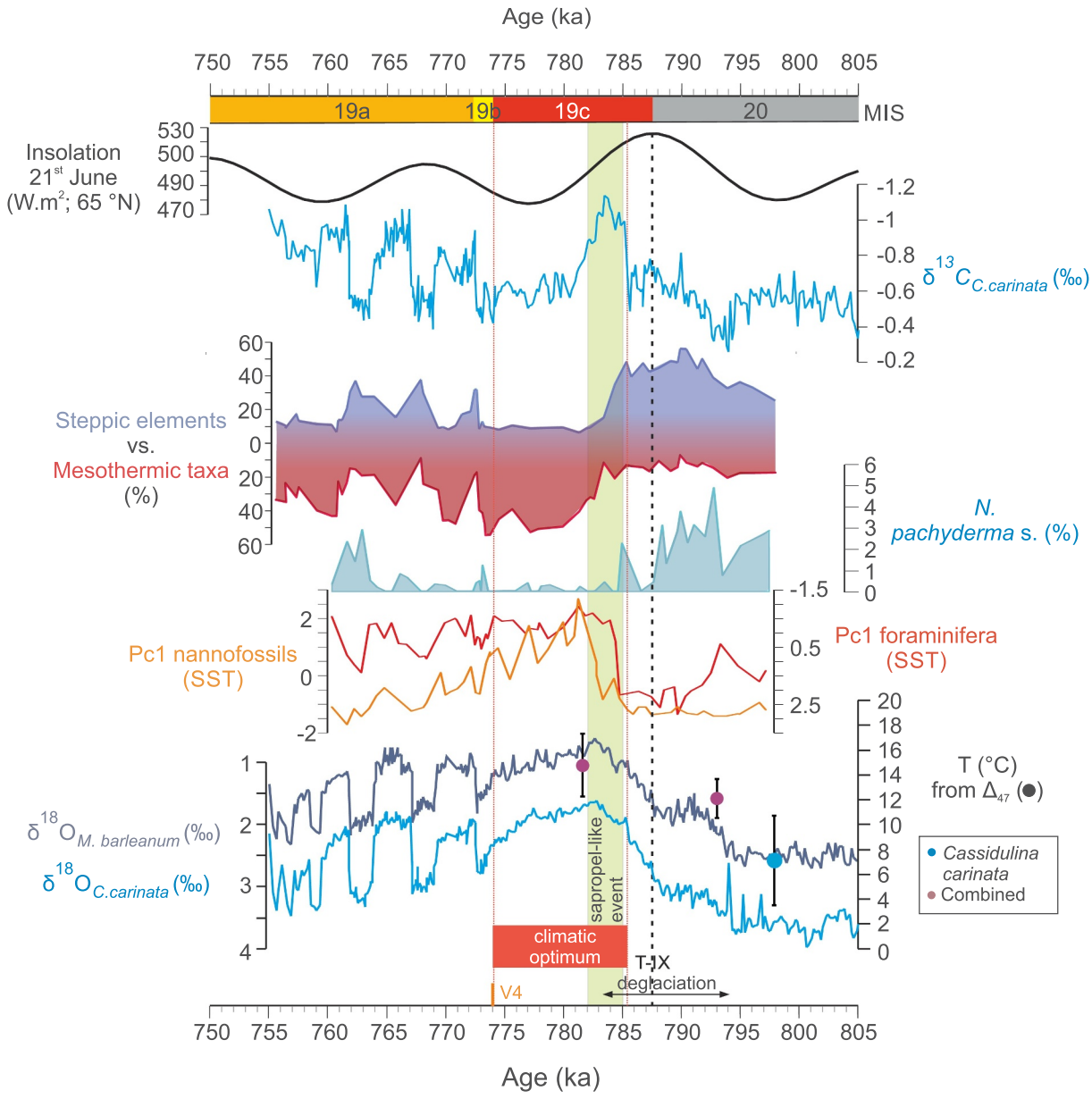

Fig. 8. Zoom on MIS 20–19 from 0.805 to 0.755 Ma, with our Δ_{47}-derived subsurface temperatures compared to high-resolution of benthic $\delta^{18}O$ and $\delta^{13}C$ curves (performed on *M. barleanum* and *C. carinnata;* Nomade et al., 2019); principal component of SST from calcareous nannofossils and foraminifera (Pc1; Maiorano et al., 2016); percentage of *N. pachyderma* left coiling (Maiorano et al., 2016), ratio mesothermic vs steppe elements (Bertini et al., 2015) and summer insolation at 65°N from Laskar et al. (2004).

notice that these $\delta^{18}O_{SW}$ reconstructions are also similar, within the limits of our error bars, to the glacial $\delta^{18}O_{SW}$ baseline (Fig. 6).

The current, annually-averaged temperatures in the Gulf of Taranto are ~ 23–24 °C at the surface and ~ 14 °C at 300 m depth (Fig. 3; Pinardi et al., 2016). Thus, temperatures recorded at the climatic optimums are comparable to modern conditions below the thermocline in the Gulf of Taranto. Furthermore, the current $\delta^{18}O_{SW}$ at 500 m depth is ~ 1.7‰, which is also similar to the reconstructed $\delta^{18}O_{SW}$ for MIS 31 and MIS 19. Interestingly, the reconstructed sub-surface temperature and $\delta^{18}O_{SW}$ during MIS 21 are was higher than the Holocene values.

7. Conclusions

By combining clumped-isotope temperature reconstructions with higher-temporal resolution proxies, we document paleoenvironmental changes over five glacial periods (MIS 36, 34, 30, 22 and 20) and three interglacials (MIS 31, 21 and 19) throughout the Mid-Pleistocene series exposed at Montalbano Ionico (Southern Italy), along the Gulf of Taranto. Over a few intervals, our data revealed large discrepancies between Mg/Ca and Δ_{47}-derived temperatures. These observations suggest that Mg/Ca-paleotemperature data may be biased, although one cannot provide any conclusive explanation about the mechanisms at play. In this work, we favoured the clumped-isotope thermometer data to reconstruct benthic (sub-surface) past seawater paleotemperatures.

During the climatic optimums of MIS 31 and MIS 19, considered as close analogues to the current interglacial in terms of insolation forcing, reconstructed sub-surface temperatures from benthic foraminifer analyses (13.8 ± 1.5 °C and 14.8 ± 1.3 °C, respectively) and $\delta^{18}O_{SW}$ are similar to the ones measured today below the thermocline in the Gulf of Taranto.

Our results show that temperature conditions were similar in all the

studied glacial periods across the MPT suggesting that oceanographic conditions in the Mediterranean Sea were relatively stable between the 41 ka-world and the 100 ka-world or that the tectonic uplift that took place at MJS during this transition balanced out the MPT cooling trend through the shallowing of the deposition site.

Declaration of competing interest

The authors declare no conflict of interest.

Acknowledgment

We gratefully thank the two anonymous reviewers for their recommendations that significantly improved the final manuscript. MP thanks G. Siani, N. Meckler, C. John, B. Malaize, T. De Garidel-Thoron and the Paleocean team from LSCE for the fruitful discussions, and A. Pereira and V. Scao for their invaluable help in the field. MP received a PhD fellowship from CEA (Commissariat a l'Energie Atomique et aux Energies Alternatives, France). All the isotopic and trace-element analyses have been performed on IRMS and ICP-MS belonging to the Analytical Platform PANOPLY (LSCE-GEOPS). The Mg/Ca measurements were financially supported by the LEFE/MAGICS project.

Appendix A. Supplementary data

Supplementary data to this article can be found online at https://doi.org/10.1016/j.palaeo.2020.109603.

References

Aiello, G., Barra, D., Parisi, R., 2015. Lower-Middle Pleistocene ostracod assemblages from the Montalbano Jonico section (Basilicata, Southern Italy). Quat. Int. 383, 47–73. Available at. https://doi.org/10.1016/j.quaint.2014.11.010.

Altenbach, A.V., Pflaumann, U., Schiebel, R., Thies, A., Timm, S., Trauth, M., 1999. Scaling percentages and distributional patterns of benthic Foraminifera with flux rates of organic carbon. J. Foraminifer. Res. 29, 173–185. Available at: http://jfr.geoscienceworld.org/content/29/3/173.abstract.

Anand, P., Elderfield, H., Conte, M.H, 2003. Calibration of Mg/Ca thermometry in planktonic foraminifera from a sediment trap time series. Paleoceanography 18 (2).

Arbuszewski, J., Demenocal, P., Kaplan, A., Farmer, E.C., 2010. On the fidelity of shell-derived d18O seawater estimates. Earth Planet. Sci. Lett. 300, 185–196. https://doi.org/10.1016/j.epsl.2010.10.035.

Balduzzi, A., Casnedi, R., Crescenti, U., Mostardini, F., Tonna, M., 1982. Il Plio-Pleistocene del sottosuolo del bacino lucano (Avanfossa appenninica). Geol. Romana 21, 89–111.

Barker, S., Greaves, M., Elderfield, H., 2003. A study of cleaning procedures used for foraminiferal Mg/Ca paleothermometry. Geochem. Geophys. Geosyst. 4, 1–20.

Bernasconi, S.M., Müller, I.A, Bergmann, K.D, Sebastian, F.M, 2018. Reducing uncertainties in carbonate clumped isotope analysis through consistent carbonate - based standardization. Geochem. Geophys. Geosyst. 19 (9), 2895–2914.

Bertini, A., Toti, F., Marino, M., Ciaranfi, N., 2015. Vegetation and climate across the Early-Middle Pleistocene transition at Montalbano Jonico, southern Italy. Quat. Int. 383, 74–88.

Bignami, F., Sciarra, R., Carniel, S., and Santoleri, R. (2007) Variability of Adriatic Sea coastal turbid waters from SeaWiFS imagery. *Journal of Geophysical Research* 112, C03S10.

Bintanja, R., Van De Wal, R.S.W., 2008. North American ice-sheet dynamics and the onset of 100,000-year glacial cycles. Nature 454, 869–872.

Bintanja, R., Van De Wal, R.S.W., Oerlemans, J., 2005. Modelled atmospheric temperatures and global sea levels over the past million years. Nature 437, 125–128.

Boussetta, S., Bassinot, F., Sabbatini, A., Caillon, N., Nouet, J., Kallel, N., Rebaubier, H., Klinkhammer, G., Labeyrie, L., 2011. Diagenetic Mg-rich calcite in Mediterranean sediments: Quantification and impact on foraminiferal Mg/Ca thermometry. *Mar. Geol.* 280, 195–204. Available at. https://doi.org/10.1016/j.margeo.2010.12.011.

Brand, W.A., Assonov, S.S., Coplen, T.B., 2010. Correction for the 17O interference in δ(13C) measurements when analyzing CO2 with stable isotope mass spectrometry (IUPAC Technical Report). Pure Appl. Chem. 82, 1719–1733. Available at: https://www.degruyter.com/view/j/pac.2010.82.issue-8/pac-rep-09-01-05/pac-rep-09-01-05.xml.

Brandimarte, L., Di Baldassarre, G., Bruni, G., D'Odorico, P., Montanari, A., 2011. Relation between the North-Atlantic Oscillation and hydroclimatic conditions in Mediterranean areas. Water Resour. Manag. 25 (5), 1269–1279.

Brilli, M., 1998. Stratigrafia isotopica del carbonio e dell'ossigeno della successione infra e mesopliocenica di Montalbano Jonico (Basilicata, Italia meridionale). Tesi di Dottorato di Ricerca in Scienze della terra XI ciclo. Università degli Studi di Roma "La Sapienza"112 pp.

Brilli, M., Lerche, L., Ciaranfi, N., Turi, B., 2000. Evidences of precession and obliquity orbital forcing in oxygen-18 isotope composition of Montalbano Jonico Section (Basilicata, southern Italy). Appl. Radiat. Isot. 52, 957–964.

Broecker, W., Peng, T.H., 1982. Tracers in the Sea, 690 pp. Palisades, N.Y, Eldigio.

Bruland, K.W., 1983. Trace elements in seawater.

Casnedi, R., 1988. La Fossa bradanica: origine, sedimentazione e migrazione. Mem. Soc. Geol. Ital. 41, 439–448.

Casnedi, R., Crescenti, U., Tonna, M., 1982. Evoluzione dell'avanfossa adriatica meridionale nel Plio-Pleistocene, sulla base di dati di sottosuolo. Mem. Soc. Geol. Ital. 24, 243–260.

Català, A., Cacho, I., Frigola, J., Pena, L.D., Lirer, F., 2019. Holocene hydrography evolution in the Alboran Sea: a multi-record and multi-proxy comparison. Clim. Past 15 (3), 927–942.

Cessi, P., Pinardi, N., Lyubartsev, V., 2014. Energetics of semienclosed basins with two-layer flows at the strait. J. Phys. Oceanogr. 44, 967–979. https://doi.org/10.1175/JPO-D-13-0129.1.

Ciaranfi N., Lirer F., Lirer L., Lourens L. J., Maiorano P., Marino M., Petrosino P., Sprovieri M., Stefanelli S., Brilli M., Girone A., Joannin S., Pelosi N. and Vallefuoco M. (2010) Integrated stratigraphy and astronomical tuning of lower-middle Pleistocene Montalbano Jonico section (southern Italy). *Quat. Int.* 219, 109–120. Available at: doi:https://doi.org/10.1016/j.quaint.2009.10.027.

Cisneros, M., Cacho, I., Frigola, J., Canals, M., Masqué, P., Martrat, B., Margaritelli, G., 2015. Sea surface temperature variability in the central-western Mediterranean Sea during the last 2700 years: a multi-proxy and multi-record approach. Clim. Past Discuss. 11, 5439–5508.

Civitarese, G., Gačić, M., Lipizer, M., Eusebi Borzelli, G.L., 2010. On the impact of the Bimodal Oscillating System (BiOS) on the biogeochemistry and biology of the Adriatic and Ionian Seas (Eastern Mediterranean). Biogeosciences 7 (12), 3987–3997.

Coletti, A.J., DeConto, R.M., Brigham-Grette, J., Melles, M., 2015. A GCM comparison of Pleistocene super-interglacial periods in relation to Lake El'gygytgyn. NE Arctic Russia. *Clim. Past* 11, 979–989.

Daëron, M., Blamart, D., Peral, M., Affek, H.P, 2016. Absolute isotopic abundance ratios and the accuracy of Δ47 measurements. Chem. Geol. 442, 83–96 ISO 690.

D'Alessandro, A., La Perna, R., Ciaranfi, N., 2003. Response of macrobenthos to changes in palaeoenvironments in the Lower–Middle Pleistocene (Lucania Basin, Southern Italy). Quat. 16, 167–183.

DeConto, R.M., Galeotti, S., Pagani, M., Tracy, D., Schaefer, K., Zhang, T., Pollard, D., Beerling, D.J., 2012. Past extreme warming events linked to massive carbon release from thawing permafrost. Nature 484 (7392), 87–91.

Eiler, J.M., 2007. "Clumped-isotope" geochemistry-the study of naturally-occurring, multiply-substituted isotopologues. Earth Planet. Sci. Lett. 262, 309–327.

Eiler, J.M., 2011. Paleoclimate reconstruction using carbonate clumped isotope thermometry. Quat. Sci. Rev. 30 (25–26), 3575–3588. https://doi.org/10.1016/j. quascirev.2011.09.001.

Elderfield, H., Yu, J., Anand, P., Kiefer, T., Nyland, B., 2006. Calibrations for benthic foraminiferal Mg/Ca paleothermometry and the carbonate ion hypothesis. Earth Planet. Sci. Lett. 250, 633–649.

Elderfield H., Greaves M., Barker S., Hall I. R., Tripati A., Ferretti P., Crowhurst S., Booth L. and Daunt C. (2010) A record of bottom water temperature and seawater d 18 O for the Southern Ocean over the past 440 kyr based on Mg/Ca of benthic foraminiferal Uvigerina spp. *Quat. Sci. Rev.* 29, 160–169. Available at: doi:https://doi.org/10.1016/j.quascirev.2009.07.013.

Emeis, K., Struck, U., Schulz, H., Rosenberg, R., Bernasconi, S., Erlenkeuser, H., Sakamoto, T., Martinez-ruiz, F., 2000. Temperature and salinity variations of Mediterranean Sea surface waters over the last 16 , 000 years from records of planktonic stable oxygen isotopes and alkenone unsaturation ratios. Palaeogeogr. Palaeoclimatol. Palaeoecol. 158 (3-4), 259–280.

Ferguson, J., Henderson, G., Kucera, M., Rickaby, R., 2008. Systematic change of foraminiferal Mg/Ca ratios across a strong salinity gradient, Earth Planet. Sci. Lett. 265, 153–166. https://doi.org/10.1016/j.epsl.2007.10.011.

Fontanier, C., Jorissen, F.J., Licari, L., Alexandre, A., Anschutz, P., Carbonel, P., 2002. Live benthic foraminiferal faunas from the Bay of Biscay: Faunal density, composition, and microhabitats. Deep. Res. Part I Oceanogr. Res. Pap. 49, 751–785.

Ghosh, P., Adkins, J., Affek, H., Balta, B., Guo, W., Schauble, E.A., Schrag, D., Eiler, J.M., 2006. 13C−18O bonds in carbonate minerals: a new kind of paleothermometer. Geochim. Cosmochim. Acta 70 (6), 1439–1456. https://doi.org/10.1016/j.gca.2005.11.014.

Giaccio, B., Regattieri, E., Zanchetta, G., Nomade, S., Renne, P.R., Sprain, C.J., Drysdale, R.N., Tzedakis, P.C., Messina, P., Scardia, G., Sposato, A., Bassinot, F., 2015. Duration and dynamics of the best orbital analogue to the present interglacial. Geology 43, 603–606.

Giorgi, F., 2006. Regional climate modeling: status and perspectives. J. Phys. IV 139, 101–118. https://doi.org/10.1051/jp4:2006139008.

Girone A., Capotondi L., Ciaranfi N., Di Leo P., Lirer F., Maiorano P., Marino M., Pelosi N. and Pulice I. (2013) Paleoenvironmental changes at the lower Pleistocene Montalbano Jonico section (southern Italy): Global versus regional signals. *Palaeogeogr. Palaeoclimatol. Palaeoecol.* 371, 62–79. Available at: doi:https://doi.org/10.1016/j.palaeo.2012.12.017.

Goudeau, M.L.S., Grauel, A.L., Tessarolo, C., Leider, A., Chen, L., Bernasconi, S.M., Versteegh, G.J.M., Zonneveld, K.A.F., Boer, W., Alonso-Hernandez, C.M., De Lange, G.J., 2014. The Glacial-interglacial transition and Holocene environmental changes in sediments from the Gulf of Taranto, central Mediterranean. Mar. Geol. 348, 88–102.

Goyet, C., Healy, R., Ryan, J., Kozyr, A., 2000. *Global distribution of total inorganic carbon and total alkalinity below the deepest winter mixed layer depths* (No. ORNL/CDIAC-127; NDP-076). Oak Ridge National Lab, TN (US).

Grauel, A.L., Schmid, T.W., Hu, B., Bergami, C., Capotondi, L., Zhou, L., Bernasconi, S.M., 2013. Calibration and application of the "clumped isotope" thermometer to foraminifera for high-resolution climate reconstructions. Geochim. Cosmochim. Acta 108, 125–140. https://doi.org/10.1016/j.gca.2012.12.049.

Gray, W.R., Weldeab, S., Lea, D.W., Rosenthal, Y., Gruber, N., Donner, B., Fischer, G., 2018. The effects of temperature, salinity, and the carbonate system on Mg/Ca in *Globigerinoides ruber* (white): A global sediment trap calibration. Earth Planet. Sci. Lett. 482, 607–620. https://doi.org/10.1016/j.epsl.2017.11.026.

Grossman, E.L., 1987. Stable isotopes in modern benthic foraminifera; a study of vital effect. J. Foraminifer. Res. 17, 48–61.

Head M. J. and Gibbard P. L. (2015) Early-Middle Pleistocene transitions: Linking terrestrial and marine realms. *Quat. Int.* 389, 7–46. Available at: doi:https://doi.org/10.1016/j.quaint.2015.09.042.

Helmke, J.P., Bauch, H.A., Erlenkeuser, H., 2003. Development of glacial and interglacial conditions in the Nordic seas between 1.5 and 0.35 Ma. Quat. Sci. Rev. 22, 1717–1728.

Hillaire-Marcel, C., De Vernal, A., McKay, J., 2011. Foraminifer isotope study of the Pleistocene Labrador Sea, northwest North Atlantic (IODP Sites 1302/03 and 1305), with emphasis on paleoceanographical differences between its "inner" and "outer" basins. Mar. Geol. 279, 188–198.

Hönisch, B., Hemming, N.G., Archer, D., Siddall, M., McManus, J.F., 2009. Atmospheric carbon dioxide concentration across the mid-Pleistocene transition. Science 324, 1551–1554. Available at: http://www.sciencemag.org/cgi/doi/10.1126/science.1171477%5Cnhttp://www.ncbi.nlm.nih.gov/pubmed/19541994.

Hurrell, J.W., 1995. Decadal trends in the north Atlantic oscillation: regional temperatures and precipitation. Science 269 (5224), 676–679.

Joannin, S., Ciaranfi, N., Stefanelli, S., 2008. Vegetation changes during the late Early Pleistocene at Montalbano Jonico (Province of Matera, southern Italy) based on pollen analysis. Palaeogeogr. Palaeoclimatol. Palaeoecol. 270, 92–101.

Kim, S.-T., O'Neil, J.R., 1997. Equilibrium and nonequilibrium oxygen isotope effects in synthetic carbonates. Geochim. Cosmochim. Acta 61, 3461–3475. Available at: http://linkinghub.elsevier.com/retrieve/pii/S0016703797001695.

Kisakürek, B., Eisenhauer, A., Böhm, F., Garbe-Schönberg, D., Erez, J., 2008. Controls on shell Mg/Ca and Sr/Ca in cultured planktonic foraminiferan, *Globigerinoides ruber* (white), Earth Planet. Sci. Lett. 273, 260–269. https://doi.org/10.1016/j.epsl.2008.06.026.

Konijnendijk, T.Y.M., Ziegler, M., Lourens, L.J., 2014. Chronological constraints on Pleistocene sapropel depositions from high-resolution geochemical records of ODP Sites 967 and 968. Newsl. Stratigr. 47, 263–282. Available at: http://openurl.ingenta.com/content/xref?genre=article&issn=0078-0421&volume=47&issue=3&spage=263.

Lang, N., Wolff, E.W, 2010. Interglacial and glacial variability from the last 800 ka in marine, ice and terrestrial archives. Clim. Past Discuss. 6, 2223–2266.

Laskar, J., Robutel, P., Joutel, F., Gastineau, M., Correia, A.C.M, Levrard, B., 2004. Astrophysics A long-term numerical solution for the insolation. Astron. Astrophys 285, 261–285.

Lea, D., Mashiotta, T., Spero, H., 1999. Controls on magnesium and strontium uptake in planktonic foraminifera determined by live culturing. Geochim. Cosmochim. Acta 63, 2369–2379. https://doi.org/10.1016/S0016-7037(99)00197-0.

Lionello, P., Malanotte-Rizzoli, P., Boscolo, R., Alpert, P., Artale, V., Li, L., Luterbacher, J., May, W., Trigo, R., Tsimplis, M., Ulbrich, U., Xoplaki, E., 2006. The Mediterranean climate: an overview of the main characteristics and issues. Dev. Earth Environ. Sci. 4 (C), 1–26.

Lisiecki, L.E., Raymo, M.E, 2005. A Pliocene-Pleistocene stack of 57 globally distributed benthic δ18O records. Paleoceanography 20 (1), 1–17.

Lourens, L.J., 2004. Revised tuning of Ocean Drilling Program Site 964 and KC01B (Mediterranean) and implications for the D 18 O, tephra, calcareous nannofossil, and geomagnetic reversal chronologies of the past 1. Paleoceanography 19 (3), 1–20 1 Myr. 19.

Maiorano, P., Capotondi, L., Ciaranfi, N., Girone, A., Lirer, F., Marino, M., Pelosi, N., Petrosino, P., Piscitelli, A., 2010. Vrica-Crotone and Montalbano Jonico sections: A potential unit-stratotype of the Calabrian Stage. Episodes 33, 218–233. Available at: http://www.scopus.com/inward/record.url?eid=2-s2.0-79957631816&partnerID=40&md5=9cd1dec5a710f096255da80208d8f766.

Maiorano, P., Bertini, A., Capolongo, D., Eramo, G., Gallicchio, S., Girone, A., Pinto, D., Toti, F., Ventruti, G., Marino, M., 2016. Climate signatures through Marine Isotope Stage 19 in the Montalbano Jonico section (Southern Italy): a land–sea perspective. Palaeogeogr. Palaeoclimatol. Palaeoecol. 461, 341–361. Available at: http://linkinghub.elsevier.com/retrieve/pii/S0031018216303819.

Marino, M., Bertini, A., Ciaranfi, N., Aiello, G., Barra, D., Gallicchio, S., Girone, A., La Perna, R., Lirer, F., Maiorano, P., Petrosino, P., Toti, F., 2015. Paleoenvironmental and climatostratigraphic insights for Marine Isotope Stage 19 (Pleistocene) at the Montalbano Jonico succession, South Italy. Quat. Int. 383, 104–115.

Mathien-Blard E. and Bassinot F. (2009) Salinity bias on the foraminifera Mg/Ca thermometry: Correction procedure and implications for past ocean hydrographic reconstructions. *Geochemistry, Geophys. Geosystems* 10.

Mcclymont, E.L., Rosell-mele, A., Haug, G.H, Lloyd, J.M, 2008. Expansion of subarctic water masses in the North Atlantic and Pacific oceans and implications for mid-Pleistocene ice sheet growth. Paleoceanography 23 (4), 1–12.

Meckler, A.N., Ziegler, M., Millán, M.I., Breitenbach, S.F.M., Bernasconi, S.M., 2014. Long-term performance of the Kiel carbonate device with a new correction scheme for clumped isotope measurements. Rapid Commun. Mass Spectrom. 28, 1705–1715.

Melles M., Melles M., Brigham-grette J., Minyuk P. S., Nowaczyk N. R., Wennrich V., Deconto R. M., Anderson P. M., Andreev A. A., Coletti A., Cook T. L., Haltia-hovi E., Kukkonen M., Lozhkin A. V, Rosén P., Tarasov P., Vogel H. and Wagner B. (2014) 2. 8 Million Years of Arctic Climate. *Science (80-.)*. 315.

Milligan, T.G., Cattaneo, A., 2007. Sediment dynamics in the western Adriatic Sea: from transport to stratigraphy. Cont. Shelf Res. 27, 287–295.

Murray, J.W., 1963. Ecological exeriments on Foraminiferida. *J. Mar. Biol. Assoc*. United Kingdom 43, 621–642.

Murray J. (2006) *Ecology and Applications of Benthic Foraminifera*. ed. Cambridge university press, United States of America by Cambridge University Press, new York.

Naafs, B.D.A., Hefter, J., Stein, R., 2013. Millennial-scale ice rafting events and Hudson Strait Heinrich (−like) Events during the late Pliocene and Pleistocene: a review. Quat. Sci. Rev. 80, 1–28.

Nomade, S., Bassinot, F., Marino, M., Simon, Q., Dewilde, F., Maiorano, P., Isguder, G., Blamart, D., Girone, A., Scao, V., Pereira, A., Toti, F., Bertini, A., Combourieu-Nebout, N., Peral, M., Bourlès, D.L., Petrosino, P., Gallicchio, S., Ciaranfi, N., 2019. High-resolution foraminifer stable isotope record of MIS 19 at Montalbano Jonico, southern Italy: a window into Mediterranean climatic variability during a low-eccentricity interglacial. Quat. Sci. Rev. 205, 106–125.

Nürnberg, D., Bijma, J., Hemleben, C., 1996. Assessing the reliability of magnesium in foraminiferal calcite as a proxy for water mass temperatures. Geochim. Cosmochim. Acta 60, 803–814. https://doi.org/10.1016/0016-7037(95)00446-7.

Oliveira, D.S.M.F., Naughton, F., Polanco-martínez, J.M., Jimenez-espejo, F.J., Grimalt, J.O., Martrat, B., Voelker, A.H.L., Trigo, R., Hodell, D.A., Abrantes, F., Desprat, S., 2017. Unexpected weak seasonal climate in the western Mediterranean region during MIS 31, a high-insolation forced interglacial nchez Go n. Quat. Sci. Rev. 161, 1–17.

Patacca, E., Scandone, P., 2004. The Plio-Pleistocene thrust belt-foredeep system in the southern Apennines and Sicily (Italy). In: *Crescenti,* et al. *(Ed.), Special Volume of the Italian Geological Society for the IGC 32 Florence 2004*. Società Geologica Italiana*, Roma*, pp. 93–129.

Peral, M., Daëron, M., Blamart, D., Bassinot, F., Dewilde, F., Smialkowski, N., Isguder, G., Jorissen, F., Kissel, C., Michel, E., Vazquez-Riveiros, N., Waelbroeck, C., 2018. Updated calibration of the clumped isotope thermometer in planktonic and benthic foraminifera. Geochimica et Cosmochimica Acta 239, 1–16.

Petrosino, P., Jicha, B.R., Mazzeo, F.C., Ciaranfi, N., Girone, A., Maiorano, P., Marino, M., 2015. The Montalbano Jonico marine succession: an archive for distal tephra layers at the Early-Middle Pleistocene boundary in southern Italy. Quat. Int. 383, 89–103.

Pinardi, N., Lyubartsev, V., Cardellicchio, N., Caporale, C., Ciliberti, S., Coppini, G., De, P.F., Dialti, L., Federico, I., Filippone, M., Grandi, A., Guideri, M., Lecci, R., Lamberti, L., Lorenzetti, G., Lusiani, P., Macripo, C.D., Maicu, F., Mossa, M., Tartarini, D., Trotta, F., Umgiesser, G., Zaggia, L., 2016. Marine Rapid Environmental Assessment in the Gulf of Taranto: a multiscale approach. Nat. Hazards Earth Syst. Sci. 16 (12), 2623–2639.

Pol K., Masson-Delmotte V., Johnsen S., Bigler M., Cattani O., Durand G., Falourd S., Jouzel J., Minster B., Parrenin F., Ritz C., Steen-Larsen H. C. and Stenni B. (2010) New MIS 19 EPICA Dome C high resolution deuterium data: Hints for a problematic preservation of climate variability at sub-millennial scale in the "oldest ice." *Earth Planet. Sci. Lett.* 298, 95–103. Available at: doi:https://doi.org/10.1016/j.epsl.2010.07.030.

Pollard, D., DeConto, R.M., 2009. Modeling West Antarctic ice sheet growth and collapse through the past five million years. Nature 458, 329–332.

Poulain, P-M. (2001) Adriatic Sea surface circulation as derived from drifter data between 1990 and 1999. *Journal of Marine Systems* 29 (1–4) (5), 3–32.

Raitzsch, M., Kuhnert, H., Groeneveld, J., Bickert, T., 2008. Benthic foraminifer Mg/Ca anomalies in South Atlantic core top sediments and their implications for paleothermometry. Geochemistry, Geophys. Geosystems 9 (5).

Regattieri E., Giaccio B., Zanchetta G., Mannella G., Nomade S., Vogel H., Tognarelli A., Boschi C., Perchiazzi N. and Galli P. (2018) Expression, frequencies and dynamics of sub-orbital scale variability during Marine Isotope Stages 19: insights from the Sulmona Basin (central Italy). In *EGU General Assembly Conference Abstracts* p. 3464.

Regattieri, E., Giaccio, B., Mannella, G., Zanchetta, G., Nomade, S., Tognarelli, A., Perchiazzi, N., Vogel, H., Boschi, C., Neil, R.D., Wagner, B., Gemelli, M., Tzedakis, P., 2019. Frequency and dynamics of millennial-scale variability during Marine Isotope Stage 19: Insights from the Sulmona Basin (central Italy). Quat. Sci. Rev. 214, 28–43.

Riley, J.P., Skirrow, G., 1975. Appendix Table 6. JP RILEY & G. SKIRROW. Chemical Oceanography 1, 561–562.

Rosenthal, Y., Perron-Cashman, S., Lear, C.H, Bard, E., Barker, S., Billups, K., Elderfield, H., 2004. Interlaboratory comparison study of Mg/Ca and Sr/Ca measurements in planktonic foraminifera for paleoceanographic research. Geochem. Geophys. Geosyst. 5 (4).

Rossignol-Strick, M., Paterne, M., 1999. A synthetic pollen record of the eastern Mediterranean sapropels of the last 1 Ma: implications for the time-scale and formation of sapropels. Mar. Geol. 153, 221–237.

Ruddiman, W.F., Raymo, M., McIntyre, A., 1986. Matuyama 41,000-year cycles: North Atlantic Ocean and northern hemisphere ice sheets. Earth Planet. Sci. Lett. 80, 117–129.

Ruddiman W. F., Sarnthein M., Backman J., Baldauf J. G., Curry W., Dupont L. M., Janecek T., Pokras E. M., Raymo M. E., Stabell B., Stein R. and Tiedemann R. (1989) Late Miocene to Pleistocene Evolution of Climate in Africa and the Low-Latitude Atlantic: Overview of Leg 108 Results. *Proc. Ocean Drill. Program, 108 Sci. Results* 108, 463–484. Available at: http://www-odp.tamu.edu/publications/108_SR/VOLUME/CHAPTERS/sr108_29.pdf.

Russell, A.D., Hönisch, B., Spero, H.J., Lea, D.W., 2004. Effects of seawater carbonate ion concentration and temperature on shell U, Mg, and Sr in cultured planktonic foraminifera. Geochim. Cosmochim. Acta 68 (21), 4347–4361. https://doi.org/10.1016/j.gca.2004.03.013.

Sabbatini A., Bassinot F., Boussetta S., Negri A., Rebaubier H., Dewilde F., Nouet J., Caillon N. and Morigi C. (2011) Further constraints on the diagenetic influences and salinity effect on *Globigerinoides ruber* (white) Mg/Ca thermometry: Implications in the Mediterranean Sea. *Geochemistry, Geophys. Geosystems* 12.

Sánchez-Goñi M. F., Llave E., Oliveira D., Naughton F., Desprat S. and Ducassou E. (2016) Climate changes in south western Iberia and Mediterranean Out fl ow variations during two contrasting cycles of the last 1 Myrs: MIS 31 – MIS. *Glob. Planet. Change* 136, 18–29. Available at: doi:https://doi.org/10.1016/j.gloplacha.2015.11.006.

Savini, A., Corselli, C., 2010. High-resolution bathymetry and acoustic geophysical data from Santa Maria di Leuca Cold Water Coral province (Northern Ionian Sea—Apulian continental slope). Deep-Sea Res. II Top. Stud. Oceanogr. 57 (5–6), 326–344.

Schauble, E.A., Ghosh, P., Eiler, J.M., 2006. Preferential formation of 13C−18O bonds in carbonate minerals, estimated using first-principles lattice dynamics. Geochim. Cosmochim. Acta 70, 2510–2529.

Scherer, R.P., Bohaty, S.M., Dunbar, R.B., Esper, O., Flores, J.A., Gersonde, R., Harwood, D.M., Roberts, A.P., Taviani, M., 2008. Antarctic records of precession-paced insolation-driven warming during early Pleistocene Marine Isotope Stage 31. Geophys. Res. Lett. 35, 1–5.

Simon, Q., Bourlès, D.L., Bassinot, F., Nomade, S., Marino, M., Ciaranfi, N., Dewilde, F., 2017. Authigenic 10Be/9Be ratio signature of the Matuyama–Brunhes boundary in the Montalbano Jonico marine succession. Earth Planet. Sci. Lett. 460, 255–267.

Stefanelli, S., 2003. Benthic foraminiferal assemblages as tools for paleoenvironmental reconstruction of the early-middle Pleistocene Montalbano Jonico composite section. BOLLETTINO-SOCIETA Paleontol. Ital. 42, 281–300.

Stefanelli, S., Capotondi, L., Ciaranfi, N., 2005. Foraminiferal record and environmental changes during the deposition of the Early-Middle Pleistocene sapropels in southern Italy. Palaeogeogr. Palaeoclimatol. Palaeoecol. 216, 27–52.

Theocharis, A., Georgopoulos, D., 1993. Dense water formation over the Samothraki and Limnos Plateaux in the north Aegean Sea (eastern Mediterranean Sea). Cont. Shelf Res. 13, 919–939.

Toti, F., 2015. Interglacial vegetation patterns at the Early-Middle Pleistocene transition: a point of view from the Montalbano Jonico section (Southern Italy). Alp. Mediterr. Quat. 28, 2015.

Trigo, R.M., Pozo-Vázquez, D., Osborn, T.J., Castro-Díez, Y., Gámiz-Fortis, S., Esteban-Parra, M.J., 2004. North Atlantic Oscillation influence on precipitation, river flow and water resources in the Iberian Peninsula. Int. J. Climatol. 24 (8), 925–944.

Tripati A. K., Eagle R. A., Thiagarajan N., Gagnon A. C., Bauch H., Halloran P. R. and Eiler J. M. (2010) 13C−18O isotope signatures and "clumped isotope" thermometry in foraminifera and coccoliths. *Geochim. Cosmochim. Acta* 74, 5697–5717. Available at: doi:https://doi.org/10.1016/j.gca.2010.07.006.

Turchetto, M., Boldrin, A., Langone, L., Miserocchi, S., Tesi, T., Foglini, F., 2007. Particle transport in the Bari Canyon (southern Adriatic Sea). Mar. Geol. 246 (2–4), 231–247.

Tzedakis P. C., Channell J. E. T., Hodell D. A., Kleiven H. F. and Skinner L. C. (2012) Determining the natural length of the current interglacial. *Nat. Geosci.* 5, 138–142. Available at: doi:https://doi.org/10.1038/ngeo1358.

de Villiers, S., Greaves, M., Elderfield, H., 2002. An intensity ratio calibration method for the accurate determination of Mg/Ca and Sr/Ca of marine carbonates by ICP-AES. Geochem. Geophys. Geosyst. 3 (1) Available at: http://doi.wiley.com/10.1029/2001GC000169.

Wagner, B., Vogel, H., Francke, A., et al., 2019. Mediterranean winter rainfall in phase with African monsoons during the past 1.36 million years. Nature 573, 256–260. https://doi.org/10.1038/s41586-019-1529-0.

Zahn, R., Pedersen, F., Bornhold, B.D., Mix, A.C., 1991. Water mass conversion in the glacial subarctic pacific (54°N, 148°W): physical constraints and the benthic- planktonic stable isotope record Rainer. Paleoceanography 6, 543–560.